

Chapter 5

Quantifying Human-Image Imitation Activities

5.1 Introduction

In this chapter, results for experiments of human-image imitation activities, described in Section 4.5.1, are presented by including time series, minimum embedding parameters, the reconstructed state spaces (RSS) using uniform time-delay embedding technique (UTDE), recurrence plots (RP), recurrent quantification analysis (RQA), and weaknesses and strengthens of RQA with three dimensional surface plots of RQA.

Time series data for this experiment are described as follows:

- Six participants defined as pN where N is the number of participant.
- Three levels of smoothness for the normalised data (sg0zmuv, sg1zmuv and sg2zmuv), computed from two different filter lengths (29 and 159) with the same polynomial degree of 5 using the function `sgolay(p,n,m)` (signal R developers, 2014),

Quantifying Human-Image Imitation Activities

- Four window lengths: 2-sec (100 samples), 5-sec (250 samples), 10-sec (500 samples) and 15-sec (750 samples), and
- Eight velocities of arm movement activity: horizontal movements in normal and faster velocity with no beat (HNnb, HFnb) and with beat (HNwb, HFwb), and vertical movements in normal and faster velocity with no beat (VNnb, VFnb) and with beat (VNwb, VFwb).

To make the visual comparison easier, time series for only three participants (*p04*, *p05*, *p10*) with a window length of 10 seconds are considered for the following results. See Appendix D for further results.

5.2 Time series

Figures 5.1 and 5.2 show time series for horizontal and vertical arm movements of participants following an image while not hearing a beat (nb) and hearing a beat (wb). Also, three levels of smoothness of normalised time series are presented (sg0, sg1 and sg2). The remaining time series are presented in Appendix D.1.

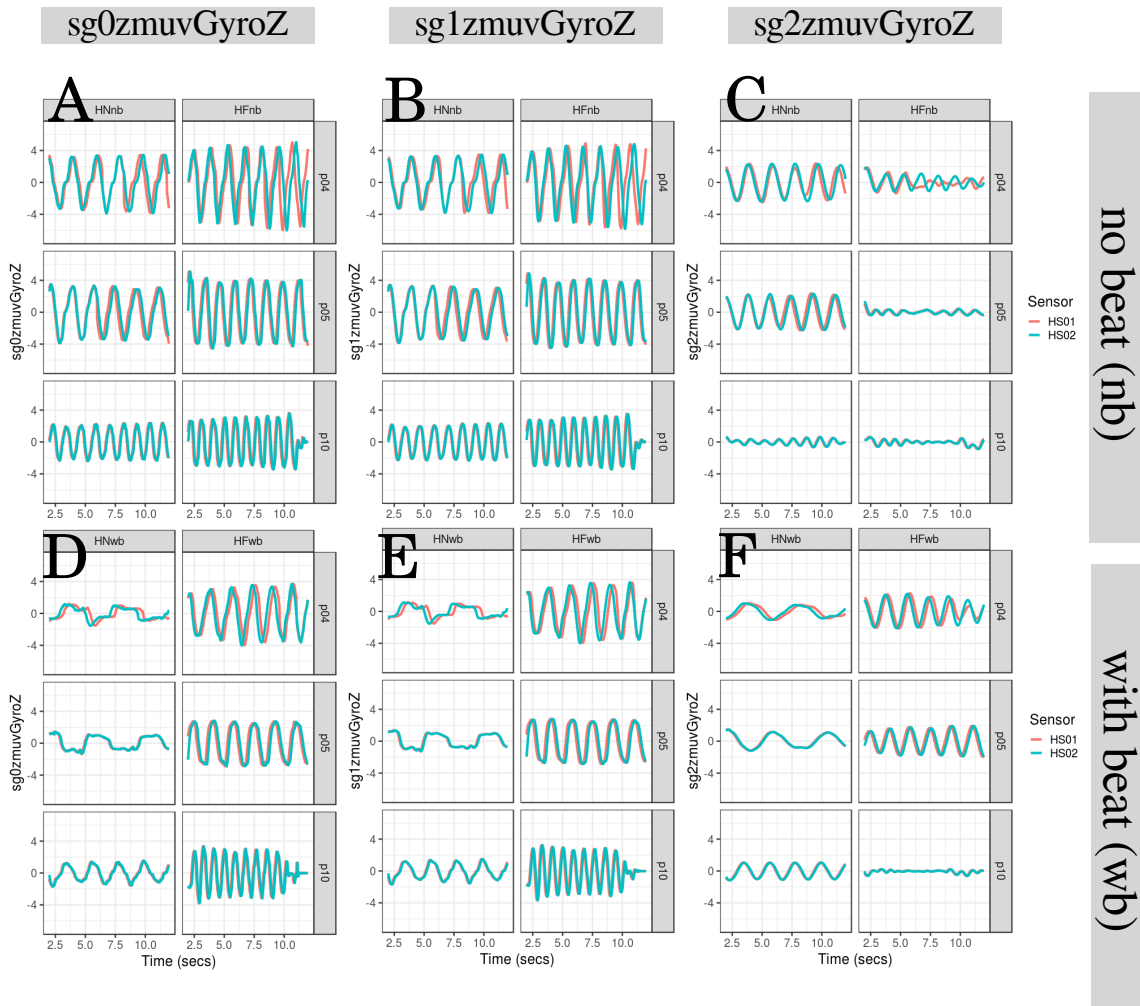


Fig. 5.1 Time series for horizontal arm movements. Time series for (A,D) raw-normalised (sg0zmuvGyroZ), (B,E) normalised-smoothed 1 (sg1zmuvGyroZ), and (C,F) normalised-smoothed 2 (sg2zmuvGyroZ). Time series are for three participants ($p04$, $p05$, and $p10$) for horizontal movements in normal and faster velocity with no beat (HNnb, HFnb) and with beat (HNwb, HFwb) using the normalised GyroZ axis (zmuvGyroZ) and two sensors attached to the participant wrist (HS01, HS02). R code to reproduce the figure is available at [\[link\]](#).

Quantifying Human-Image Imitation Activities

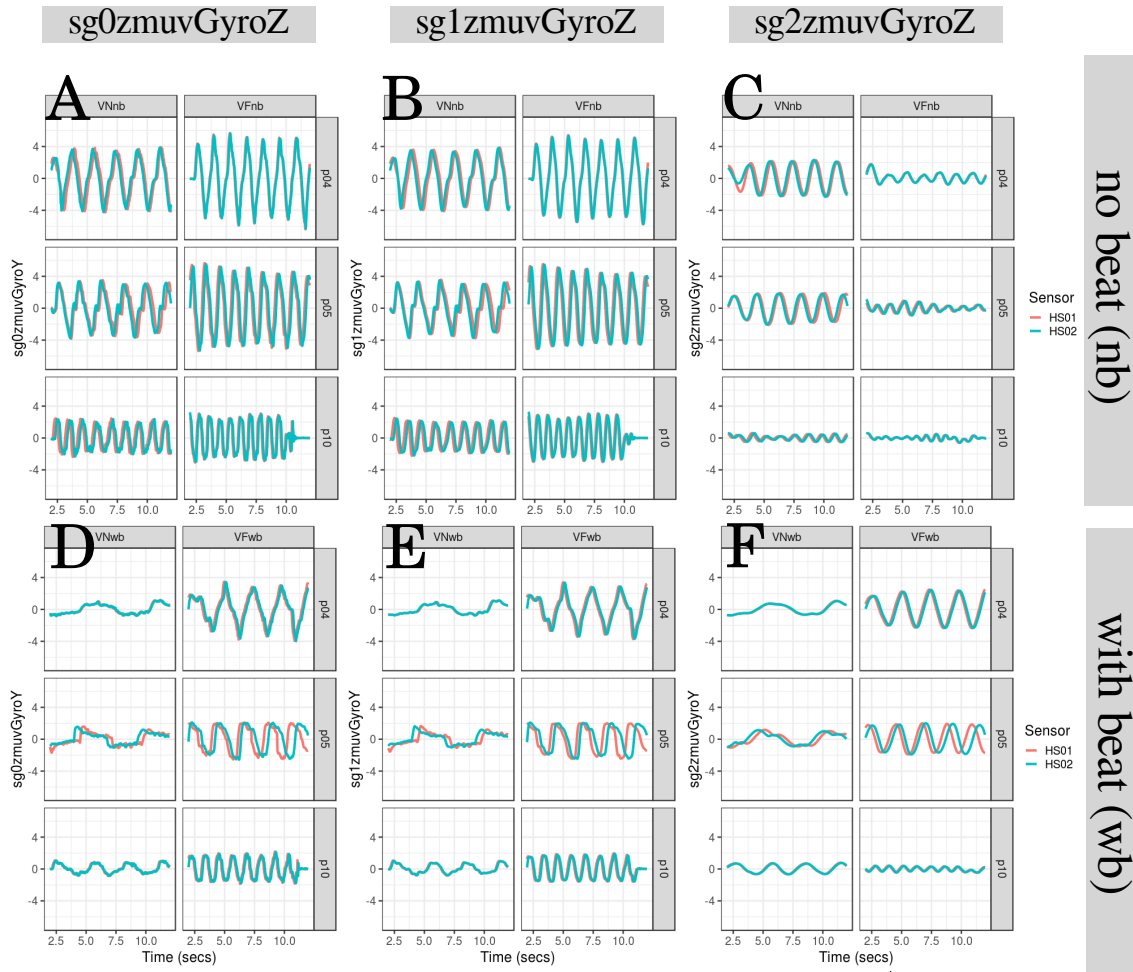


Fig. 5.2 Time series for vertical arm movements. Time series for (A,D) raw-normalised (sg0zmuvGyroY), (B,E) normalised-smoothed 1 (sg1zmuvGyroY), and (C,F) normalised-smoothed 2 (sg2zmuvGyroY). Time series are for three participants ($p04$, $p05$, and $p10$) for vertical movements in normal and faster velocity with no beat (VNnb , VFnb) and with beat (VNwb , VFwb) using the normalised GyroY axis (zmuvGyroY) and two sensors attached to the participant wrist (HS01, HS02). R code to reproduce the figure is available at [🔗](#).

5.3 Minimum Embedding Parameters

The first step to create Reconstructed State Spaces (RSSs) with the use of Uniform Time-Delay Embedding (UTDE) is to compute the average minimum embedding parameters for all participants, sensors and activities using False Nearest Neighbour (FNN) and Average Mutual Information (AMI) algorithms.

Hence, Figs. 5.3 illustrate the box plots for minimum embedding dimensions. For horizontal arm movements (Figs. 5.3(A)), one can notice how the interquartile range appear to be near to one independently of the activity or sensor. With regards to the level of smoothness, there is a decrease of sample mean (gray rhombus) as the smoothness increase. Similarly, for vertical arm movements (Figs. 5.3(B)) the interquartile range of activities and sensors appears to be near to one. In addition to that, the increase of smoothness is affected by a decrease in sample means (gray rhombus) meaning that there is a decrease of dimensionality of the dynamics of the time series data. For further details of the minimum dimension values see Figs ??, ??, ?? and ?? in Appendix D.2.

Figs. 5.4 illustrate the box plots for first minimum AMI. Box plots for horizontal arm movements (Figs. 5.4(A)) for HNwb appear more spread (interquartile range between 10 to 20) while other activities there is a slight variation of values (interquartile range between 5 to 10). Little can be said regardless the sample mean of each axis (gray rhombus) which is not proportionally affected as the smoothed of the time series increase. Box plots for vertical arm movements (Figs. 5.4(B)) show that the interquartile range of each activity is constant except for the activity VFwb. Additionally, the increase of smoothness of time series (sg0 to sg2) made the sample mean (gray rhombus) to increase which means that the maximal information to knowledge from $x(n)$ to $x(t + \tau_0)$ also increase. For further details of the minimum dimension values see Figs D.11, D.12, D.13 and D.14 in Appendix D.2.

Quantifying Human-Image Imitation Activities

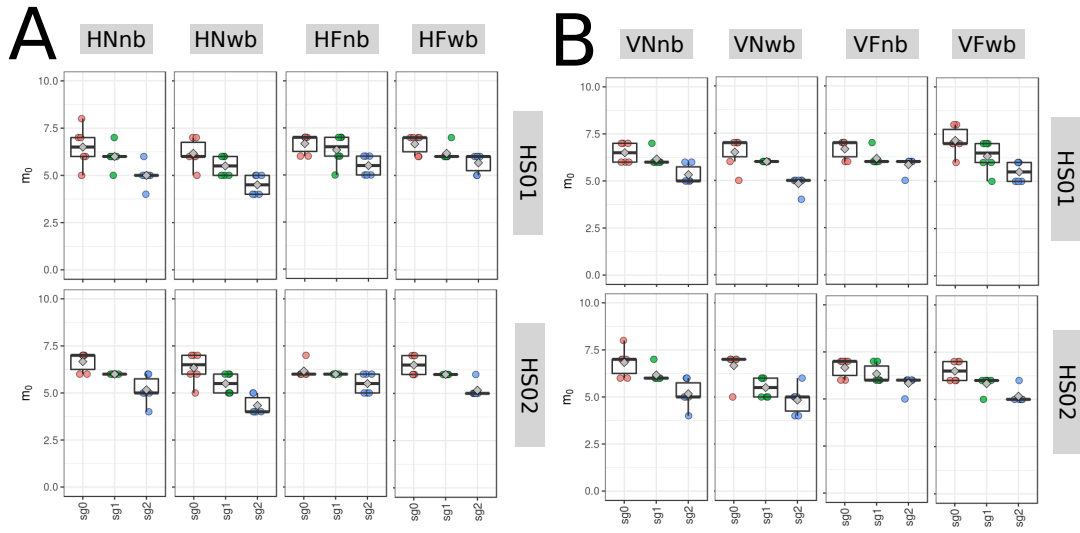


Fig. 5.3 Box plots for minimum embedding dimensions. Box plots of minimum embedding dimensions for (A) horizontal and (B) vertical arm movements for normal and faster velocity (N/F) with no beat (nb) and with beat (wb) movements using sensors 01 and 02 attached to the wrist of the participant (HS01, HS02). Minimum embedding dimensions are for six participants ($p01, p04, p05, p10, p11, p15$) with three smoothed signals (sg0, sg1 and sg2) and window length of 10 seconds. R code to reproduce the figure is available at [\[link\]](#).

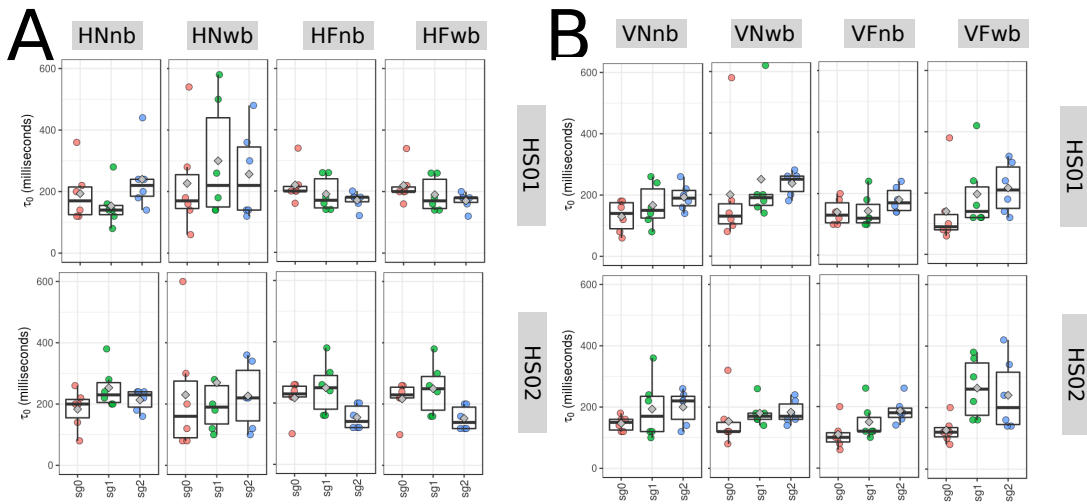


Fig. 5.4 Box plots for 1st minimum AMI. Box plots of the 1st minimum AMI values for (A) horizontal and (B) vertical arm movements for normal and faster velocity (N/F) with no beat (nb) and with beat (wb) movements using sensors 01 and 02 attached to the wrist of the participant (HS01, HS02). First minimum AMI values in milliseconds are for six participants ($p01, p04, p05, p10, p11, p15$) with three smoothed signals (sg0, sg1 and sg2) and window length of 10 seconds. R code to reproduce the figure is available at [\[link\]](#).

5.3.1 Average minimum embedding parameters

Although the implementation of Uniform Time-Delay Embedding (UTDE) is simple, the main challenge is the selection of appropriate embedding parameters to reconstruct the state spaces of each time series as these are unique in terms of its structure (modulation of amplitude, frequency and phase) (Bradley and Kantz, 2015; Frank et al., 2010; Samà et al., 2013). With that in mind, one problem that this thesis has faced is the selection of embedded parameters that can represent all time series. The solution to that problem was to compute a sample mean over all values for all participants, activities and sensors (Section 3.4.3). Hence, the average minimum embedding parameters is computed with a sample mean of $\bar{m}_0 = 6$ from the minimum values of $E_1(m)$ in Figs 5.3 and a sample mean of $\bar{\tau}_0 = 10$ from minimum values of AMIs in Figs 5.4. Hence, Reconstructed State Spaces (RSSs), Recurrence Plots (RPs) and Recurrence Quantification Analysis (RQA) metrics are computed with the average minimum embedding parameters ($\bar{m}_0 = 6$, $\bar{\tau}_0 = 10$).

5.4 Reconstructed state spaces with UTDE

Reconstructed state spaces for horizontal normal and horizontal faster arm movements with no beat are shown in Fig 5.5. The smoothness of the time series show a slightly change of smoothed trajectories in the RSSs for sg0zmuvGyroZ and sg1zmuvGyroZ, while the RSSs trajectories for sg2zmuvGyroZ appear to be distorted (Fig 5.5). One can see slightly differences in the RSSs trajectories when comparing sensors HS01 and HS02 for horizontal normal arm movement with no beat (Fig 5.5(A, B)) and horizontal faster arm movements with no beat (Fig 5.5(C, D)). With regards to the type of movement, the RSSs trajectories appear to change little when comparing horizontal normal with faster arm movements (Fig 5.5).

Quantifying Human-Image Imitation Activities

Fig 5.6 shows trajectories of the reconstructed state space for horizontal normal and horizontal faster arm movements while beat sounds. Hence, as in Fig 5.5, it can also be noted in Fig 5.6 that the smoothness of sg0zmuvGyroZ and sg1zmuvGyroZ appear to affect little the RSSs trajectories, while RSSs trajectories for sg2zmuvGyroZ substantially change so as to show different patterns. However, the trajectories in the RSS appear to change little when comparing the differences between the type of sensors HS01 and HS02 (Fig 5.6). For the type of movements, trajectories show differences for horizontal normal and horizontal faster arm movements (Fig 5.6).

Fig 5.7 show trajectories for reconstructed state spaces of vertical normal and vertical faster arm movements with no beat. Smoothness of the RSSs trajectories is slightly noticed for sg0zmuvGyroY and sg1zmuvGyroY, whereas RSSs trajectories for sg2zmuvGyroY are evidently different (Fig 5.7). When comparing the RSSs trajectories from sensors HS01 and HS02, it can be noted little change, whereas the comparison from type of movement, the trajectories difference is more notable (Fig 5.7).

Fig 5.8 show trajectories for reconstructed state space of vertical normal and vertical faster arm movements for participants hearing a beat. Smoothness of RSSs trajectories appear to show slightly differences between sg0zmuvGyroY and sg1zmuvGyroY, however RSSs trajectories for sg2zmuvGyroY are different (Fig 5.8). With regards to the type of sensor HS01 and HS02, RSSs trajectories appear to change little, whereas for type of activity of normal and faster arm movements, RSSs trajectories show evidently differences (Fig 5.8).

5.4 Reconstructed state spaces with UTDE

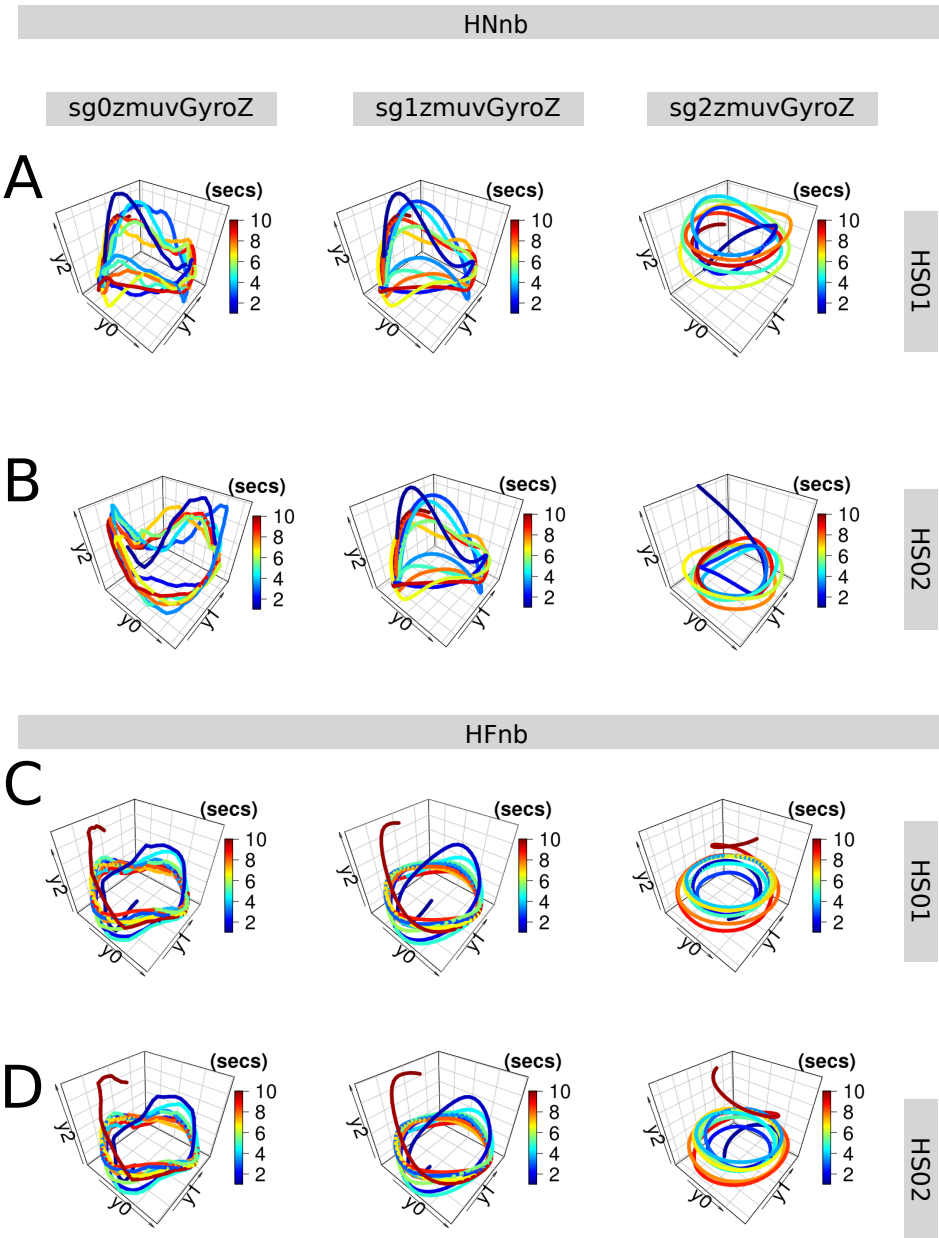


Fig. 5.5 RSSs for horizontal arm movements (no beat). Reconstructed state spaces of participant p01 for (A, B) horizontal normal movements with no beat (HNnb) and (C, D) horizontal faster velocity with no beat (HFnb). Time series for raw-normalised (sg0zmuvGyroZ), normalised-smoothed 1 (sg1zmuvGyroZ) and normalised-smoothed 2 (sg2zmuvGyroZ) with (A, C) sensor attached to the participant (HS01), and (B, D) sensor attached to the participant (HS02). Reconstructed state spaces were computed with embedding parameters $\bar{m}_0 = 6$, $\bar{\tau}_0 = 10$. R code to reproduce the figure is available at [\[link\]](#).

Quantifying Human-Image Imitation Activities

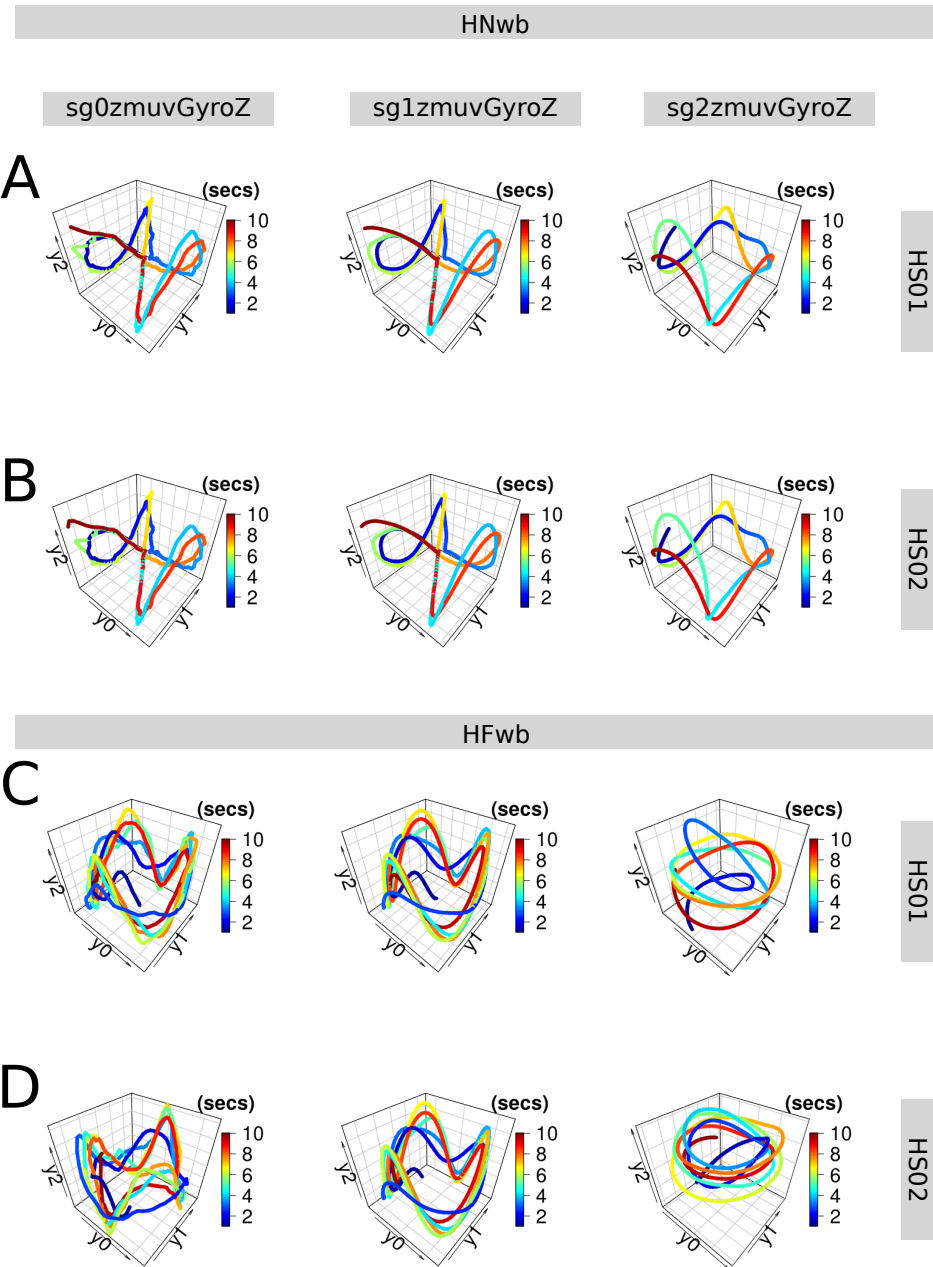


Fig. 5.6 RSSs for horizontal arm movements (with beat). Reconstructed state spaces of participant p01 for (A, B) horizontal normal movements with beat (HNwb) and (C, D) horizontal faster velocity with beat (HFwb). Time series for raw-normalised ($sg0zmuvGyroZ$), normalised-smoothed 1 ($sg1zmuvGyroZ$) and normalised-smoothed 2 ($sg2zmuvGyroZ$) with (A, C) sensor attached to the participant (HS01), and (B, D) sensor attached to the participant (HS02). Reconstructed state spaces were computed with embedding parameters $\bar{m}_0 = 6$, $\bar{\tau}_0 = 10$. R code to reproduce the figure is available at [\[link\]](#).

5.4 Reconstructed state spaces with UTDE

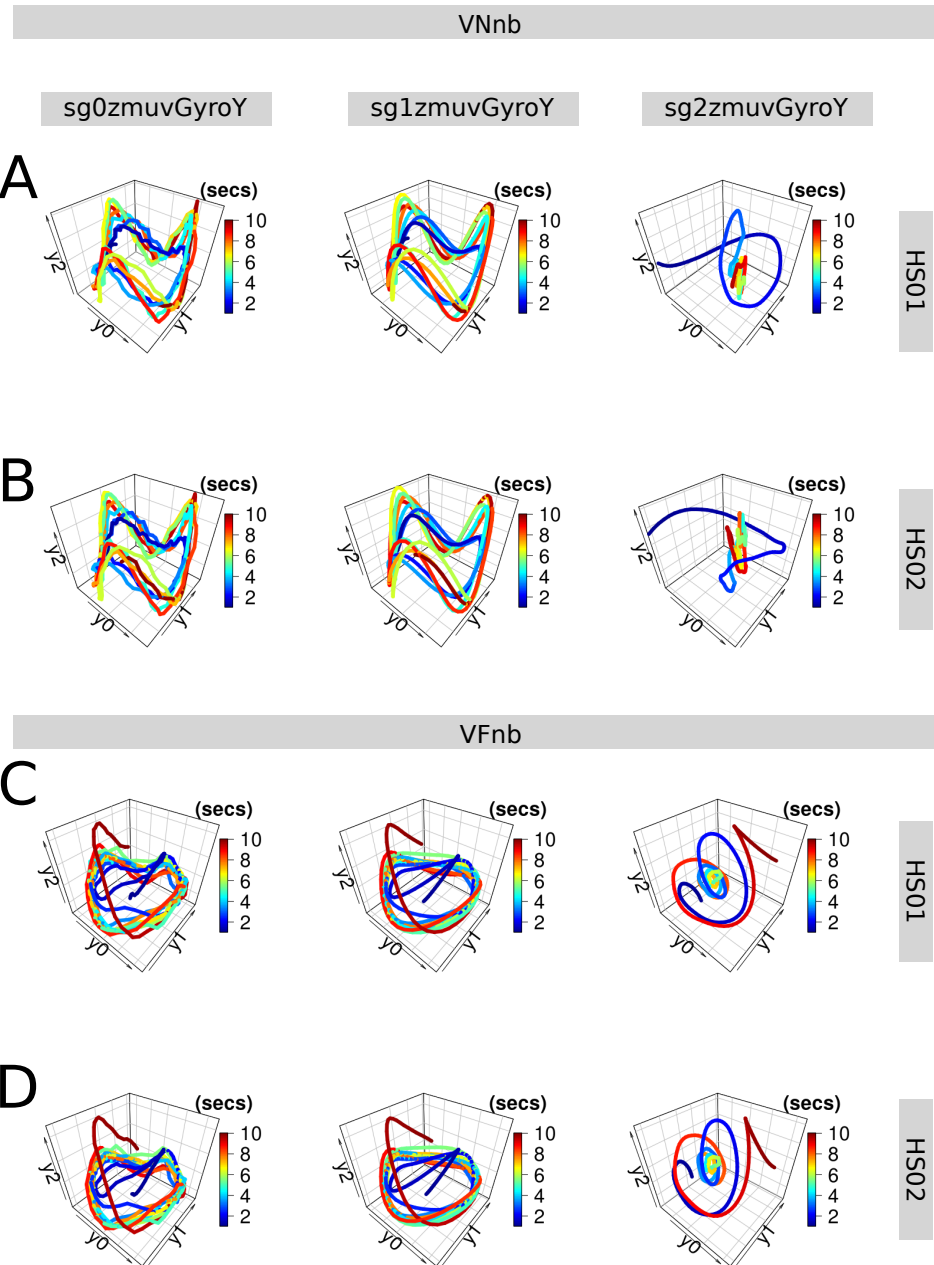


Fig. 5.7 RSSs for vertical arm movements (no beat). Reconstructed state spaces of participant p01 for (A, B) vertical normal movements with no beat (VNnb) and (C, D) vertical faster velocity with no beat (VFnb). Time series for raw-normalised ($sg0zmuvGyroY$), normalised-smoothed 1 ($sg1zmuvGyroY$) and normalised-smoothed 2 ($sg2zmuvGyroY$) with (A, C) sensor attached to the participant (HS01), and (B, D) sensor attached to the participant (HS02). Reconstructed state spaces were computed with embedding parameters $\bar{m}_0 = 6$, $\bar{\tau}_0 = 10$. R code to reproduce the figure is available at [\[link\]](#).

Quantifying Human-Image Imitation Activities

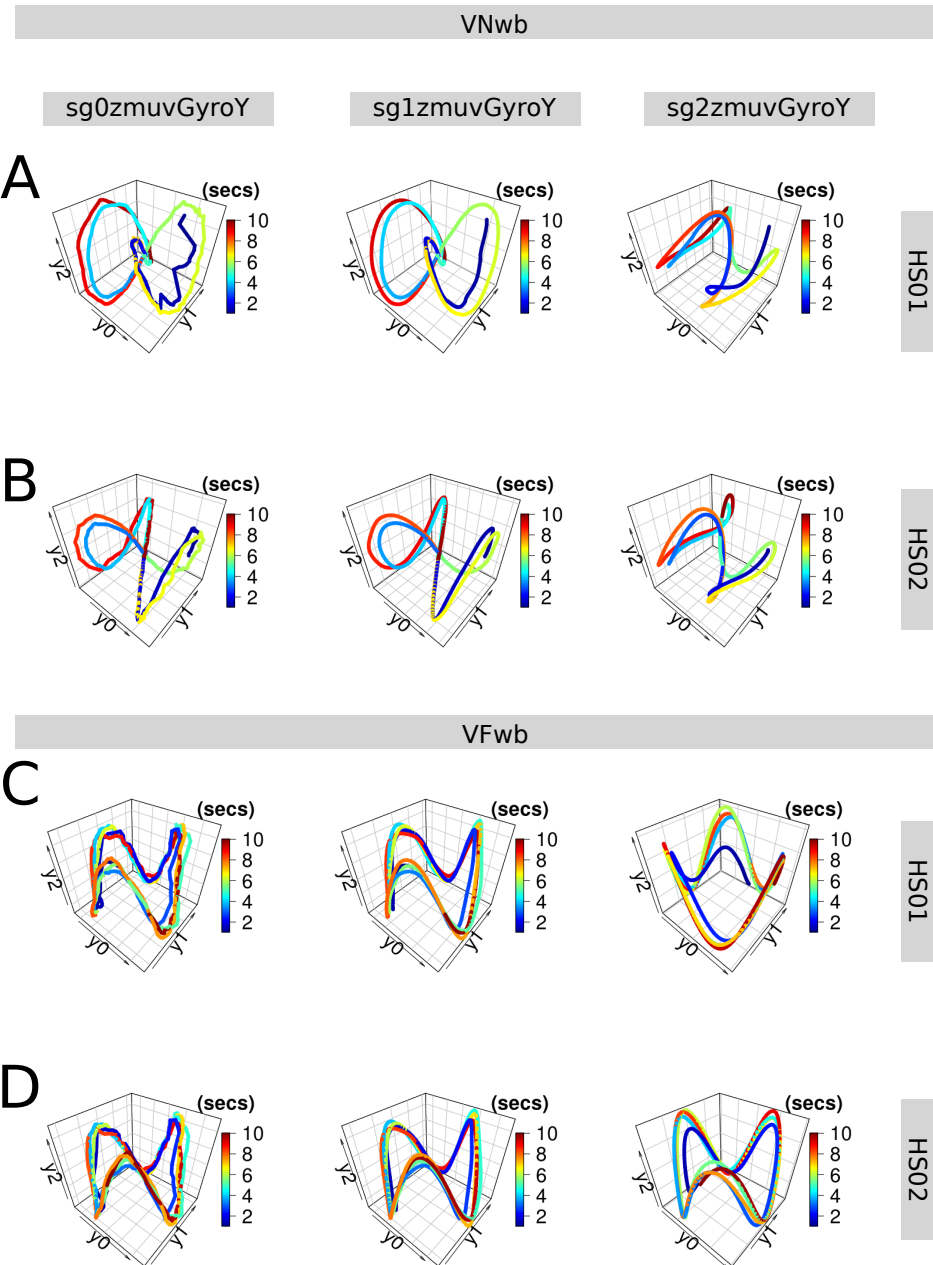


Fig. 5.8 RSSs for vertical arm movements (with beat). Reconstructed state spaces of participant p01 for (A, B) vertical normal movements with beat (VNwb) and (C, D) vertical faster velocity with beat (VFwb). Time series for raw-normalised ($sg0zmuvGyroY$), normalised-smoothed 1 ($sg1zmuvGyroY$) and normalised-smoothed 2 ($sg2zmuvGyroY$) with (A, C) sensor attached to the participant (HS01), and (B, D) sensor attached to the participant (HS02). Reconstructed state spaces were computed with embedding parameters $\bar{m}_0 = 6$, $\bar{\tau}_0 = 10$. R code to reproduce the figure is available at [\[db\]](#).

5.5 Recurrences Plots

Patterns of recurrence plots (RPs) are described in this section. Recurrence plots are computed with embedding parameters $\overline{m_0} = 6$, $\overline{\tau_0} = 10$ and a recurrence threshold $\epsilon = 1$ for participant *p01* performing horizontal and vertical arm movements in normal and faster velocity with beat and no beat sound (Figs 5.9, 5.10, 5.11 and 5.12).

Figs 5.9 show recurrence plots for horizontal normal and horizontal faster arm movements with no beat sound. For horizontal normal arm movements with no beat, patterns in RPs for sg0zmuvGyroZ and sg1zmuvGyroZ look similar, however patterns in RPs for sg2zmuvGyroZ are different, such behavior of RPs patterns is similar with regards to the smoothness presented in horizontal and faster arm movements with beat (Fig 5.10). With regards to the type of sensor, there is little visual differences in RPs patters, while patterns of RPs for different activities present diagonal lines that appear to be closer and more dense for horizontal faster arm movement than horizontal normal arm movements (Fig 5.9).

Figs 5.10 show patterns of RPs for horizontal normal and faster arm movements while participants listen to a beat. For these patterns in the RPs, the type activities for normal and faster arm movements can be easily noticed in the patterns, as well as the change of smoothness between sg0zmuvGyroZ and sg1zmuvGyroZ with the patterns for sg2zmuvGyroZ. It can also noted that there is little visual differences between the RP patters for sensor HS01 and HS02.

Figs 5.11 show patterns of RPs for vertical normal and faster arm movements while no hearing a beat. One can note the evidently differences of patterns between the levels of smoothness where, for instance, patterns of RPs from sg0zmuvGyroY and sg1zmuvGyroY looks similar while RPs for sg2zmuvGyroY are completely black. Similarly, one can see little visual changes when comparing RPs patterns between

Quantifying Human-Image Imitation Activities

sensors HS01 and HS02. However, the RPs patterns create a more dense presence of diagonal lines for faster arm movements than for normal arm movements.

Figs 5.12 show RPs patterns for vertical normal and faster arm movements for participants hearing a beat. Patterns of RP for vertical normal and vertical faster arm movements are visually noticeable as well as RPs patterns for changes in the increase of smoothness between sg0zmuvGyroY and sg1zmuvGyroY and with sg2zmuvGyroY. One can also note that there is little visual changes of RPs patterns from different sensors.

5.5 Recurrences Plots

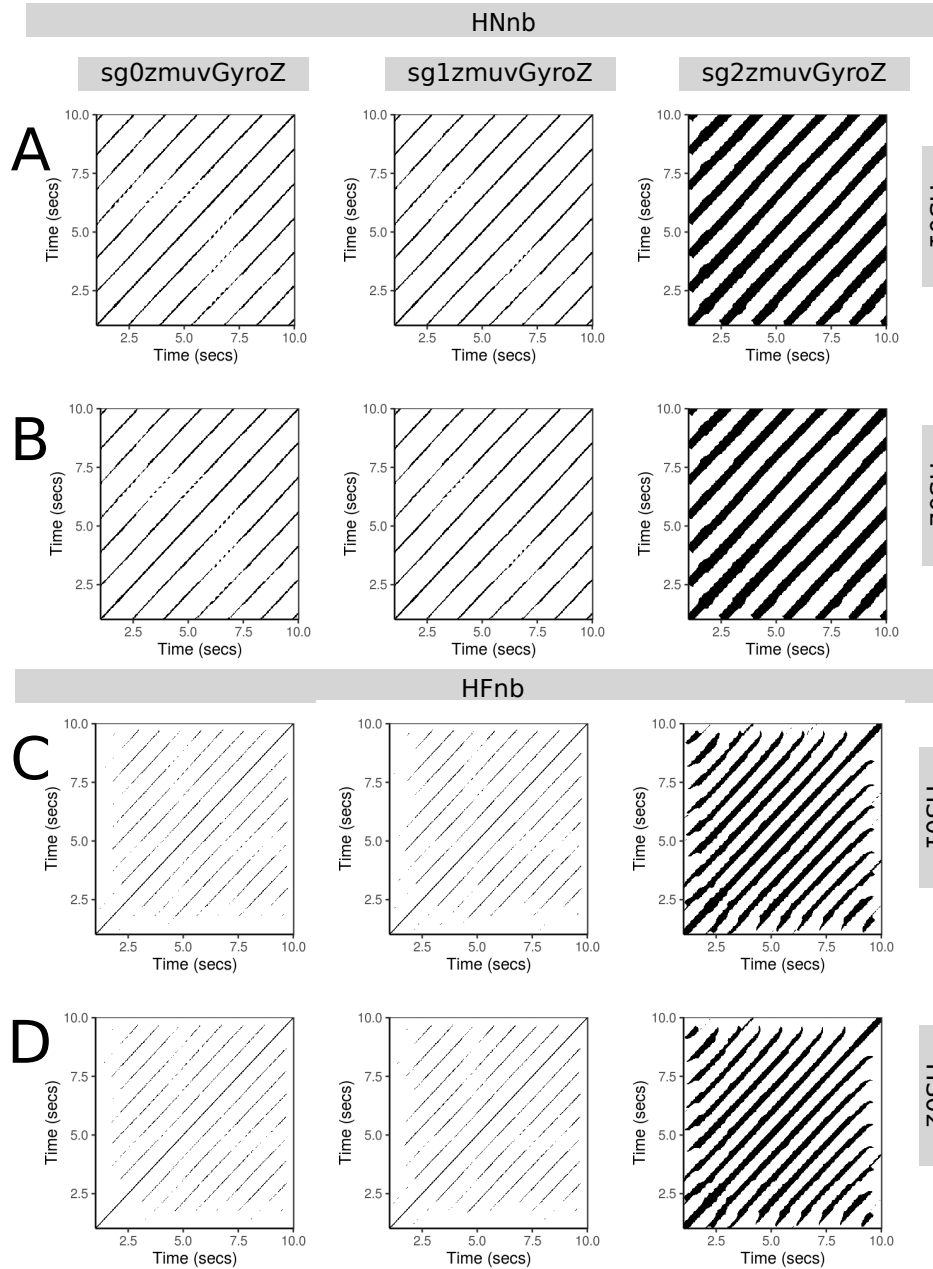


Fig. 5.9 RPs for horizontal arm movements (no beat). Recurrence plots of participant p01 for (A, B) horizontal normal movements with no beat (HNnb) and (C, D) horizontal faster movements with no beat (HFnb). Time series for raw-normalised ($sg0zmuvGyroZ$), normalised-smoothed 1 ($sg1zmuvGyroZ$) and normalised-smoothed 2 ($sg2zmuvGyroZ$) with (A, C) sensor 01 attached to the participant (HS01), and (B, D) sensor 02 attached to the participant (HS02). Recurrence plots were computed with embedding parameters $\bar{m}_0 = 6$, $\bar{\tau}_0 = 10$ and recurrence threshold $\epsilon = 1$. R code to reproduce the figure is available at [\[link\]](#).

Quantifying Human-Image Imitation Activities

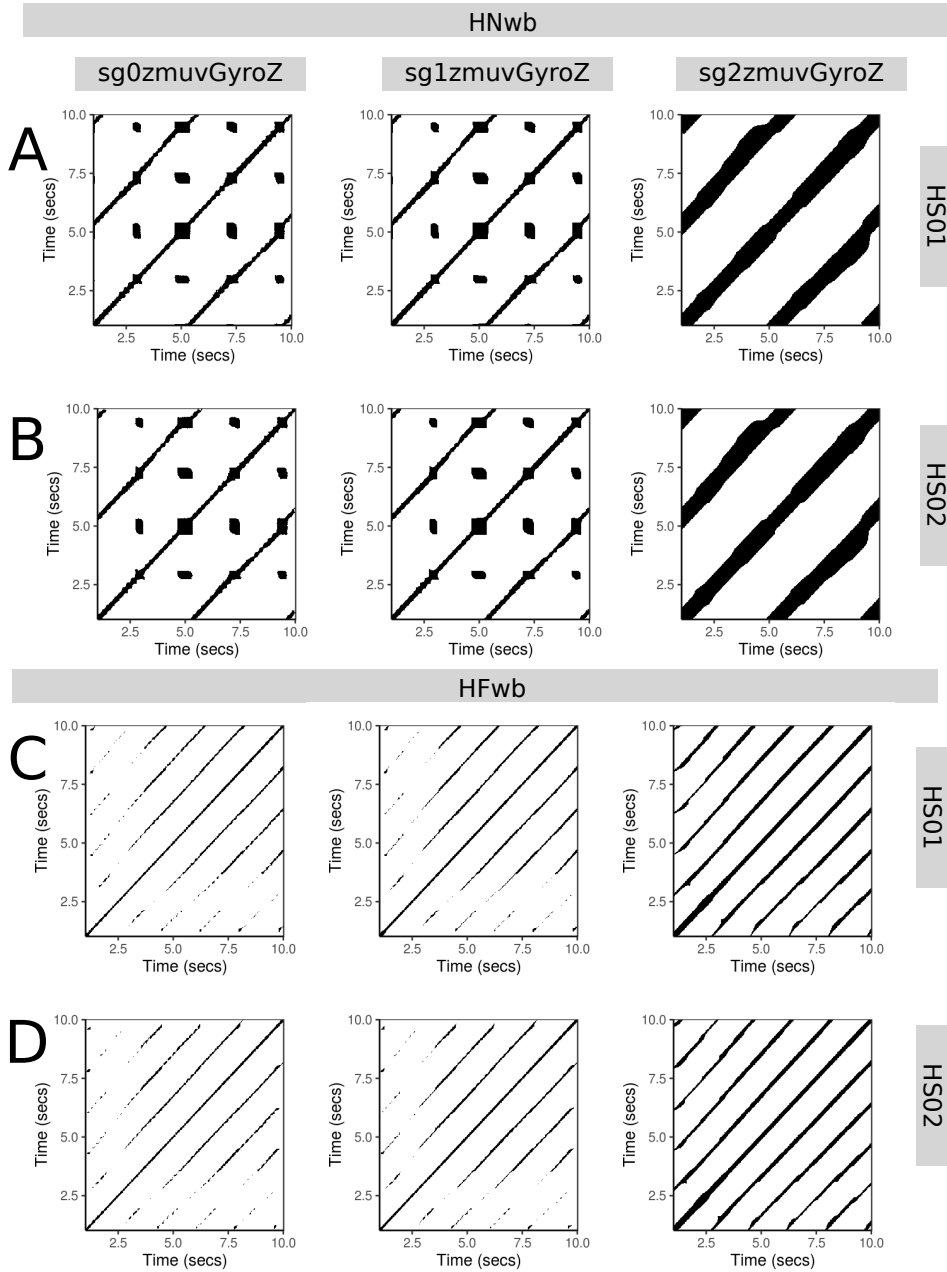


Fig. 5.10 RPs for horizontal arm movements (with beat). Recurrence plots of participant p01 for (A, B) horizontal normal movements with beat (HNwb) and (C, D) horizontal faster movements with beat (HFwb). Time series for raw-normalised (sg0zmuvGyroZ), normalised-smoothed 1 (sg1zmuvGyroZ) and normalised-smoothed 2 (sg2zmuvGyroZ) with (A, C) sensor 01 attached to the participant (HS01), and (B, D) sensor 02 attached to the participant (HS02). Recurrence plots were computed with embedding parameters $\bar{m}_0 = 6$, $\bar{\tau}_0 = 10$ and recurrence threshold $\epsilon = 1$. R code to reproduce the figure is available at [\[link\]](#).

5.5 Recurrences Plots

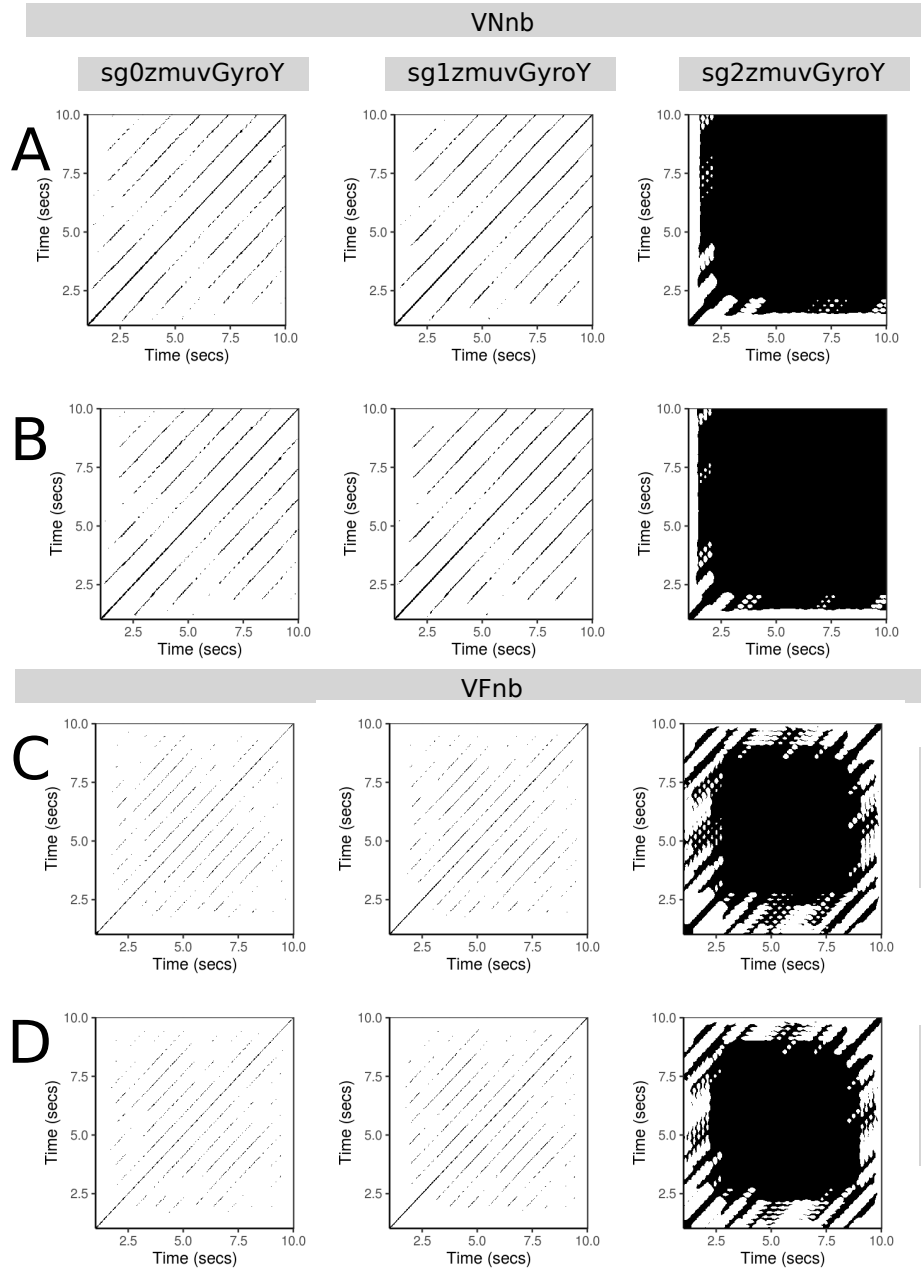


Fig. 5.11 RPs for vertical arm movements (no beat). Recurrence plots of participant p01 for (A, B) vertical normal movements with no beat (VNnb) and (C, D) vertical faster movements with no beat (VFnb). Time series for raw-normalised ($sg0zmuvGyroY$), normalised-smoothed 1 ($sg1zmuvGyroY$) and normalised-smoothed 2 ($sg2zmuvGyroY$) with (A, C) sensor 01 attached to the participant (HS01), and (B, D) sensor 02 attached to the participant (HS02). Recurrence plots were computed with embedding parameters $\bar{m}_0 = 6$, $\bar{\tau}_0 = 10$ and recurrence threshold $\epsilon = 1$. R code to reproduce the figure is available at [\[link\]](#).

Quantifying Human-Image Imitation Activities

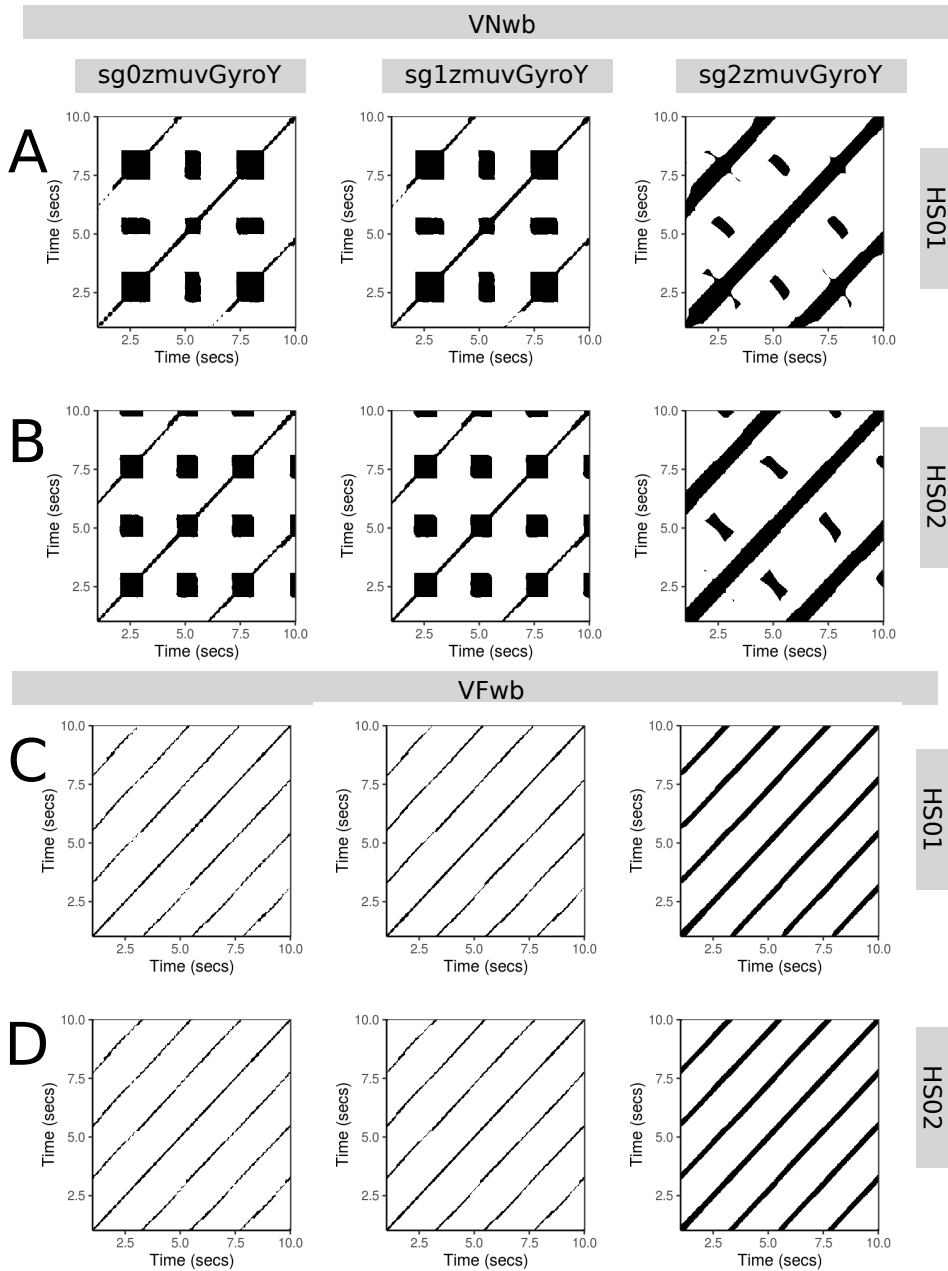


Fig. 5.12 RPs for vertical arm movements (with beat). Recurrence plots of participant p01 for (A, B) vertical normal movements with beat (VNwb) and (C, D) vertical faster movements with beat (VFwb). Time series for raw-normalised ($sg0zmuvGyroY$), normalised-smoothed 1 ($sg1zmuvGyroY$) and normalised-smoothed 2 ($sg2zmuvGyroY$) with (A, C) sensor 01 attached to the participant (HS01), and (B, D) sensor 02 attached to the participant (HS02). Recurrence plots were computed with embedding parameters $\bar{m}_0 = 6$, $\bar{\tau}_0 = 10$ and recurrence threshold $\epsilon = 1$. R code to reproduce the figure is available at [\[link\]](#).

5.6 Recurrence Quantification Analysis

In this section is shown Recurrence Quantification Analysis (RQA) metrics (REC, DET, RATIO and ENTR) of six participants ($p01, p04, p05, p10, p11, p15$) for horizontal arm movements (HNnb, HNwb, HFnb, HFwb) and vertical arm movements (VNnb, VNwb, VFnb, VFwb) with sensors HS01 and HS02, and three smoothed time series (sg0zmuvgyro, sg1zmuvgyro and sg2zmuvgyro). I hence compute four metrics of RQA metrics (REC, DET, RATIO and ENTR) with embedding parameters $\overline{m_0} = 6$, $\overline{\tau_0} = 10$ and recurrence threshold $\epsilon = 1$.

REC values

Figs 5.13(A) and 5.14(A) show box plots of REC values, representing % of black dots in the RPs, for horizontal arm movements and vertical arm movements. In figs 5.13(A) can be noted that the interquartile range for sg2 is greater than the sg0 and sg1 for activities HNnb and HFnb, while REC values for activities HNwb and HFwb appear to increase its sample mean (gray rhombus) as the smoothness increase. Similarly, in figs 5.14(A) can be seen that there is a large interquartile range for sg2 in activities with no beat (VNnb, VFnb), while activities with beat (VNwb and VFwb) appear to be increase its sample mean (gray rhombus) as the smoothness of the time series increase. REC values from sensors HS01 and HS02 appear to differ little for both horizontal and vertical arm movements. For further details of individual REC values of participants, see Figs D.27 and D.28 in Section D.5.

DET values

DET values, representing predictability and organisation of the RPs, appear to be constant irregardless of the source of time series (Figs 5.13(B) and 5.14(B)). However,

Quantifying Human-Image Imitation Activities

it can be noted a slight increase of DET values as the smoothness increase. For further details of individual DET values of participants, see Figs D.29, D.30 in Section D.5.

RATIO values

RATIO values, representing dynamics transitions, for horizontal and vertical arm movements are shown in Figs 5.13(C) and 5.14(C). In Figs 5.13(C), for vertical arm movements, can be noted that HNwb activity present the less interquartile range while other seem to have similar interquartile range. Also, the increase of smoothness makes RATIO values to decrease (see gray rhombus). Similarly, in Figs 5.14(C), for vertical arm movements, is shown that VNwb has the less interquartile range as well as sg2 for VFnb and VFwb activities. The increase of smoothness of time series affect in the way that the sample mean values of RATIO values (gray rhombus) decrease. For further details of individual DET values of participants, see Figs D.31, D.32 in Section D.5.

ENTR values

Figs 5.13(D) and 5.14(D) show ENTR values, representing the complexity of the structure of time series, for horizontal and vertical arm movements. Generally, figs 5.13(D) and 5.14(D) illustrate that the increase of smoothness causes an increase of sample mean (gray rhombus) of ENTR values in each of the activities and sensors. For both vertical and horizontal ENTR values for Nwb seems to be a bit higher than Nnb, while Fnb and Fwb appear to have similar values. Also, there is little change between HS01 and HS02 sensors. For further details of individual ENTR values of participants, see Figs D.33, D.34 in Section D.5.

5.6 Recurrence Quantification Analysis

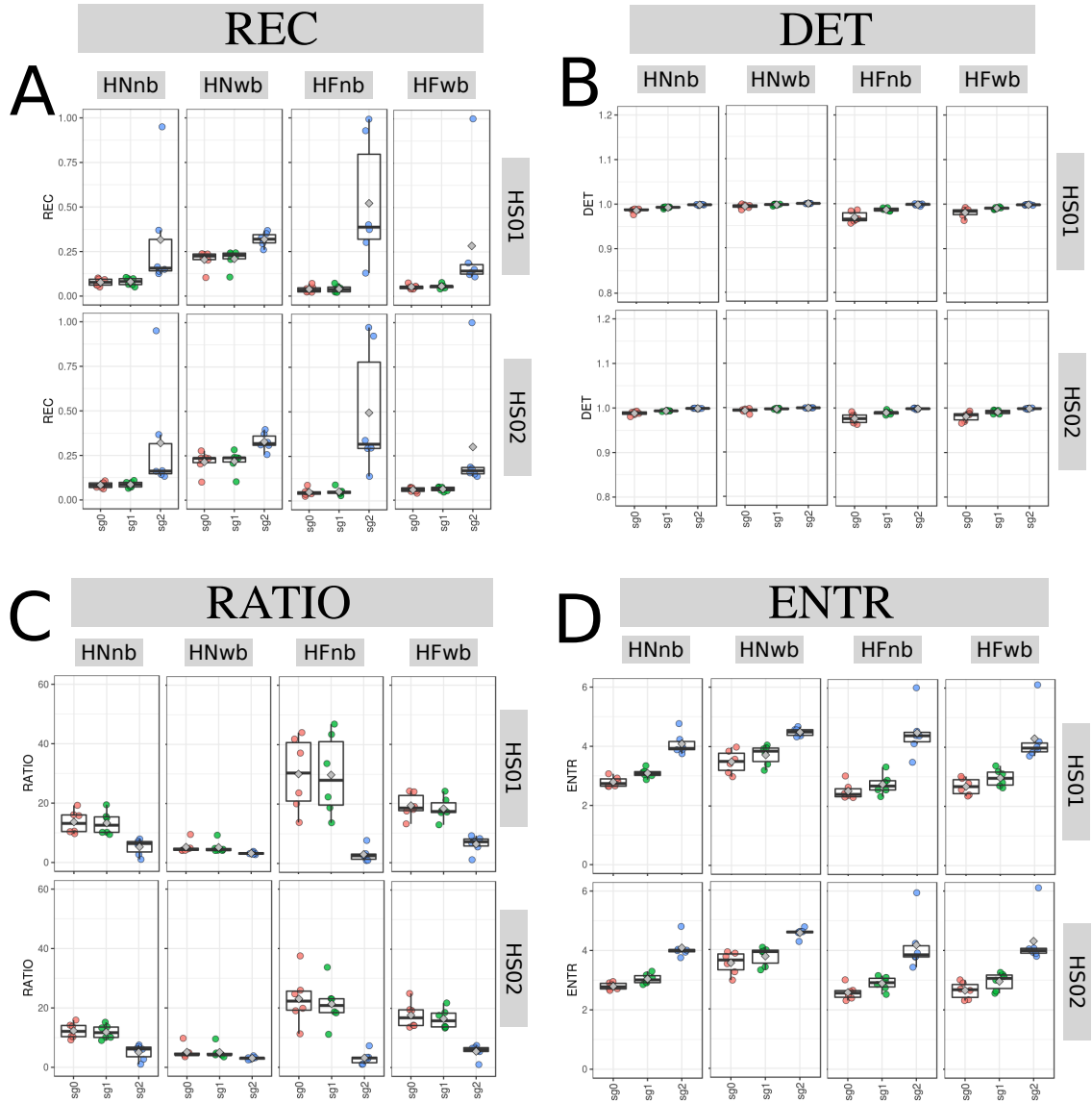


Fig. 5.13 Box plots of RQA values for horizontal arm movements. Box plots of (A) REC, (B) DET, (C) RATIO, and (D) ENTR values for 6 participants performing HNnb, HNwb, HFnb and HFwb movements with sensors HS01, HS02 and three smoothed-normalised time series (sg0, sg1 and sg2). RQA values were computed with embedding parameters $\bar{m}_0 = 6$, $\bar{\tau}_0 = 10$ and recurrence threshold $\epsilon = 1$. R code to reproduce the figure is available at [\[link\]](#).

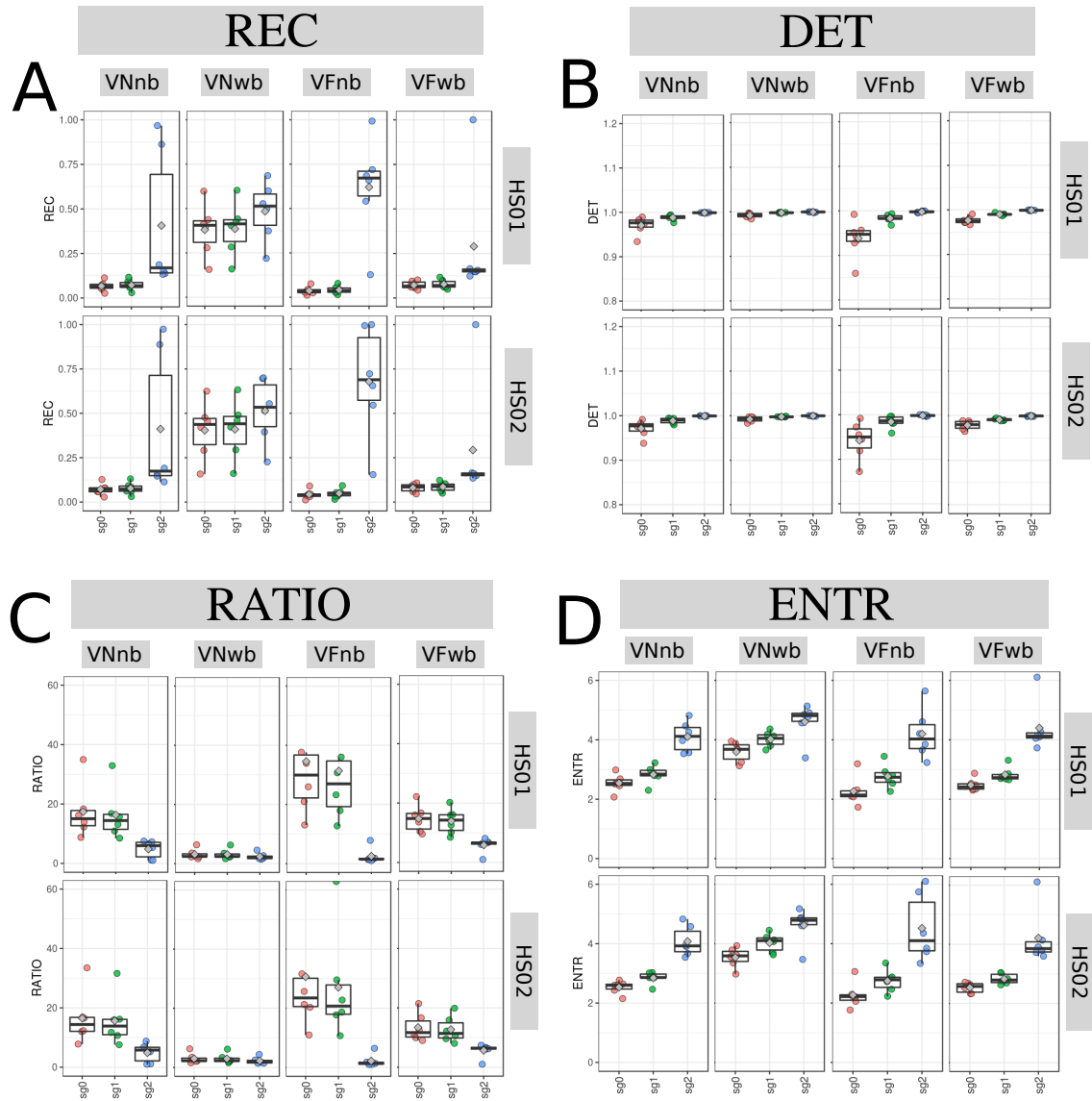


Fig. 5.14 Box plots for RQA values for vertical arm movements. Box plots of (A) REC, (B) DET, (C) RATIO, and (D) ENTR values for 6 participants performing VNnb, VNwb, VFnb and VFwb movements with sensors HS01, HS02 and three smoothed-normalised time series (sg0, sg1 and sg2). RQA values were computed with embedding parameters $\bar{m}_0 = 6$, $\bar{\tau}_0 = 10$ and recurrence threshold $\epsilon = 1$. R code to reproduce the figure is available at [\[R\]](#).

5.7 Weaknesses and strengths of RQA

Surfaces for RQA metrics (REC, DET, RATIO, ENTR) are computed with the variation of embedding values by an increase of one ($0 \leq m \leq 10$, $0 \leq \tau \leq 10$) and recurrence thresholds by an increase of 0.1 ($0.2 \geq \epsilon \leq 3$). Hence, different characteristics of 3D surface plots of RQA are shown by considering different activities, sensors, window lengths and level of smoothness and participants.

Figs 5.15 show the 3D surface plots for RQA metrics (REC, DET, RATIO, ENTR) using time series of participant *p01*, sensor HS01, activity HNb, sg0zmuvGyroZ axis and a 10 seconds window length. The 3D surface plot of REC values, representing the % of recurrence dots in the RP, show highest values of REC when embedding values are near to 1 and the recurrence threshold is at the maximum ($\epsilon = 3$ for this surface plot). Similarly, it can be seen a decrease of REC values as the embedding dimension and embedding delay values increase, however there is an increase of REC values as the recurrence threshold is increasing (Fig 5.15(A)). Regarding the 3D surface plots of DET values, representing predictability and organisation of the RPs, Fig 5.15(B) show slightly uniform values when varying both embedding parameters and recurrence threshold with the exception of embedding parameters near to 1 and recurrence thresholds near to 0.2 where the DET values are smaller. 3D surface for RATIO values, representing dynamic transitions, show a plateau with low values recurrence threshold values greater than 1.0. However, there is a fluctuated increase of RATIO values as the embedding values increase given that the recurrence threshold is lower than 1 (Fig 5.15(C)). For ENTR values, representing the complexity of the structure of the time series, Fig 5.15(D) show a maximum value of ENTR when embedding parameters are near to 1 and recurrence threshold values are near to 3.0. It can also be noted fluctuations in the 3D surface when ENTR values are greater than 2.5 (red surface) for embedding dimensions between 3 to 9 and a decrease of ENTR values per each embedding dimension for

Quantifying Human-Image Imitation Activities

delay embedding values (yellow surface). Additionally, ENTR values decrease as the embedding dimension and delay embedding decrease.

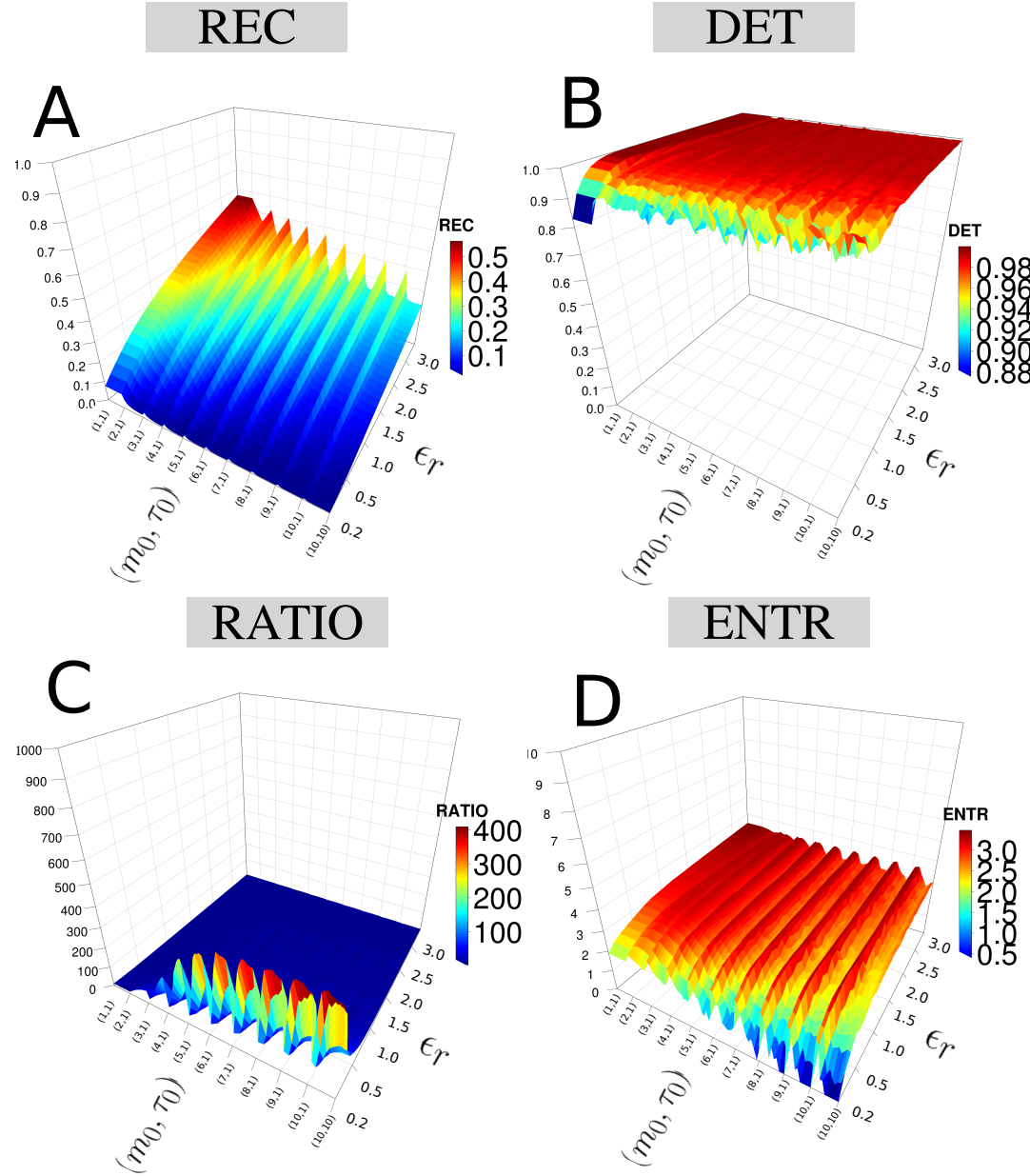


Fig. 5.15 3D surface plots of RQA metrics. 3D surface plots of RQA metrics (A) REC, (B) DET, (C) RATIO and (D) ENTR with an increasing pair of embedding parameters ($0 \leq m_0 \leq 10$, $0 \leq \tau_0 \leq 10$) and recurrence thresholds ($0.2 \leq \epsilon_r \leq 3$). RQA metrics are computed with the time series of participant *p01* using HS01 sensor, HNb activity, sg0zmuvGyroZ axis and 10 seconds for window length. R code to reproduce the figure is available at [DOI](#).

5.7.1 Sensors and activities

Figs 5.16 and 5.17 show 3D surface plots of RQA metrics (REC, DET, RATIO, ENTR) for horizontal arm movements (HNnb, HNwb, HFnb, HFwb) using sensor HS01 and HS02 for participant *p01* with sg0zmuvGyroZ axis and 10 seconds window length. Hence, Figs 5.16 present 3D surface plots of RQA metrics for HS01, where 3D surface plots of REC values (Fig 5.16(A)) appear to be similar across the activities (HNnb, HFnb, HFwb) with the exception of HNwb which decrease of REC values is mainly affected by the increase of recurrence threshold and slightly affected to the increase of embedding dimension parameters. For DET values, 3D surface plots in Figs 5.16(B) appear to show values near to 1.0 (red colour surface), however HNwb shown fluctuations of DET values as the embedding dimension increase, it can also be noted a decrease of DET values for certain values of recurrence threshold (2.6 for HNwb, 0.3 for HFnb, and 0.3 for HFwb). For Fig 5.16(C)), 3D surface plots of RATIO values appear to be similar, showing a plateau for values between 0 to 50 (blue surface) and the increase of peaks is different for each of the activities. For Fig 5.16(D), ENTR values present different surface formations, for instance, HNnb show fluctuated higher values of ENTR (red colour surface), whereas for activity HNwb the ENTR values are higher (red colour surface) for recurrence threshold near to 3.0, ENTR values for HFnb appear to be higher when embedding dimension is near to 10, while higher values for ENTR values for HFwb appear to be when the recurrence threshold is near to 0.2.

Then, looking and comparing visually one by one of the 3D surface plots for sensors HS01 and HS02 in Figs 5.16 and 5.17, one can notice little differences in the shape of the surface plots. Similarly, there is little variations in the surface plots for vertical arm movements with the sensors HS01 and HS02 (Figs 5.18 and 5.19).

With regards to horizontal and vertical movements, 3D surface plots appear to be similar for REC, DET and RATIO values with sensor HS01 (Figs 5.16 and 5.18) and

Quantifying Human-Image Imitation Activities

sensor HS02 (Figs 5.17 and 5.19), however 3D surface plots of ENTR values in each of the arm movements presents distinguishable variations in the surface plots, see Figs 5.16(D) and 5.18(D) for horizontal and vertical arm movements with sensor HS01 and Figs 5.17(D) and 5.19(D) for horizontal and vertical arm movements with sensor HS02.

5.7 Weaknesses and strengths of RQA

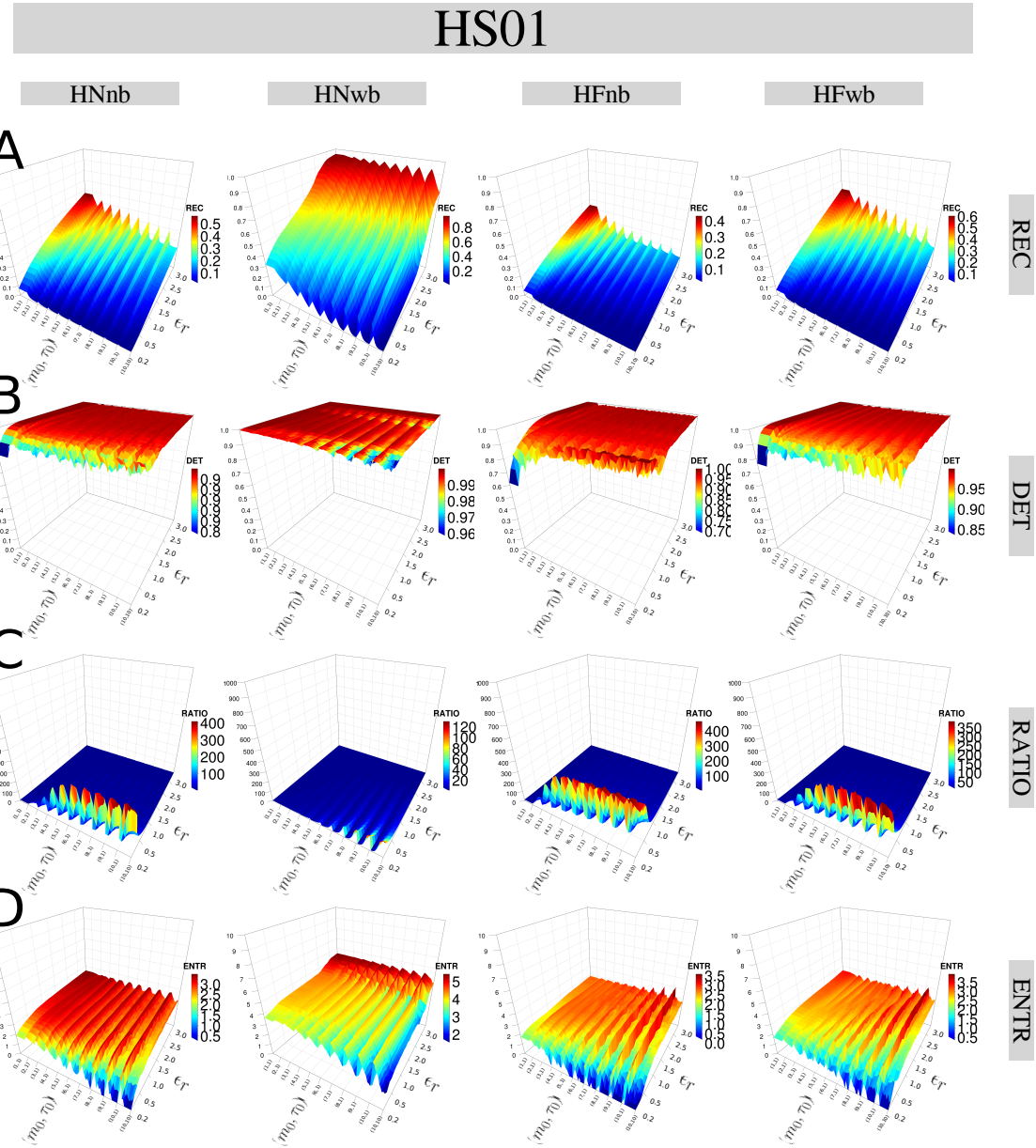


Fig. 5.16 3D surface plots of RQA metrics for horizontal arm movements with HS01. 3D surface plots for (A) REC, (B) DET, (C) RATIO and (D) ENTR values with increasing pair of embedding parameters ($0 \leq m \leq 10$, $0 \leq \tau \leq 10$) and recurrence thresholds ($0.2 \leq \epsilon \leq 3$). RQA metrics are computed with the time series of participant p01 for sensors HS01, horizontal arm movement activities (HNnb, HNwb, HFnb, HFwb) and sg0zmuvGyroZ axis with 10 seconds window length. R code to reproduce the figure is available at [\[link\]](#).

Quantifying Human-Image Imitation Activities

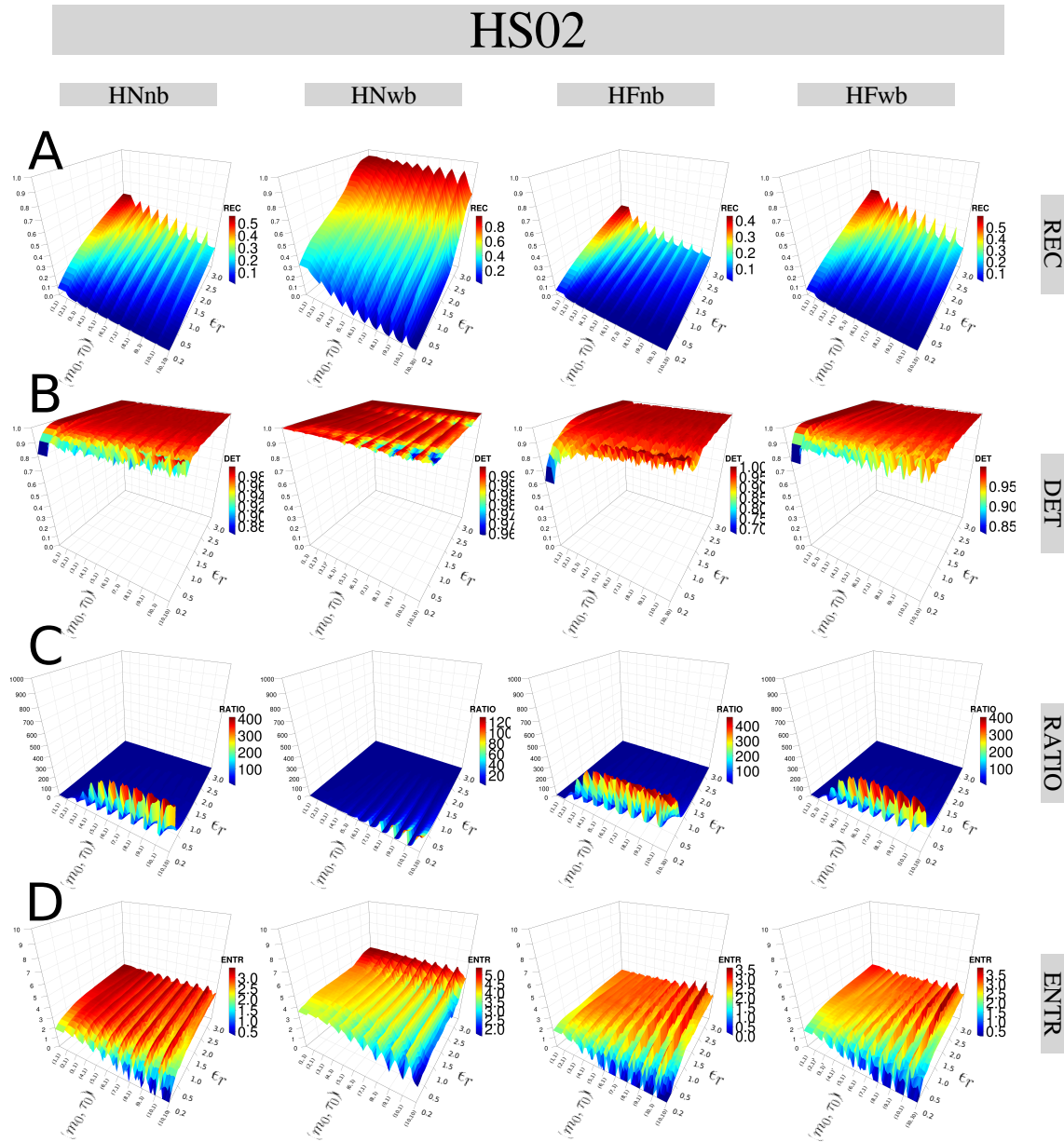


Fig. 5.17 3D surface plots of RQA metrics for horizontal arm movements with HS02. 3D surface plots for (A) REC, (B) DET, (C) RATIO and (D) ENTR values with increasing pair of embedding parameters ($0 \leq m \leq 10$, $0 \leq \tau \leq 10$) and recurrence thresholds ($0.2 \leq \epsilon \leq 3$). RQA metrics are computed with the time series of participant p01 for sensors HS02, horizontal arm movement activities (HNnb, HNwb, HFnb, HFwb) and sg0zmuvGyroZ axis with 10 seconds window length. R code to reproduce the figure is available at [\[GitHub\]](#).

5.7 Weaknesses and strengths of RQA

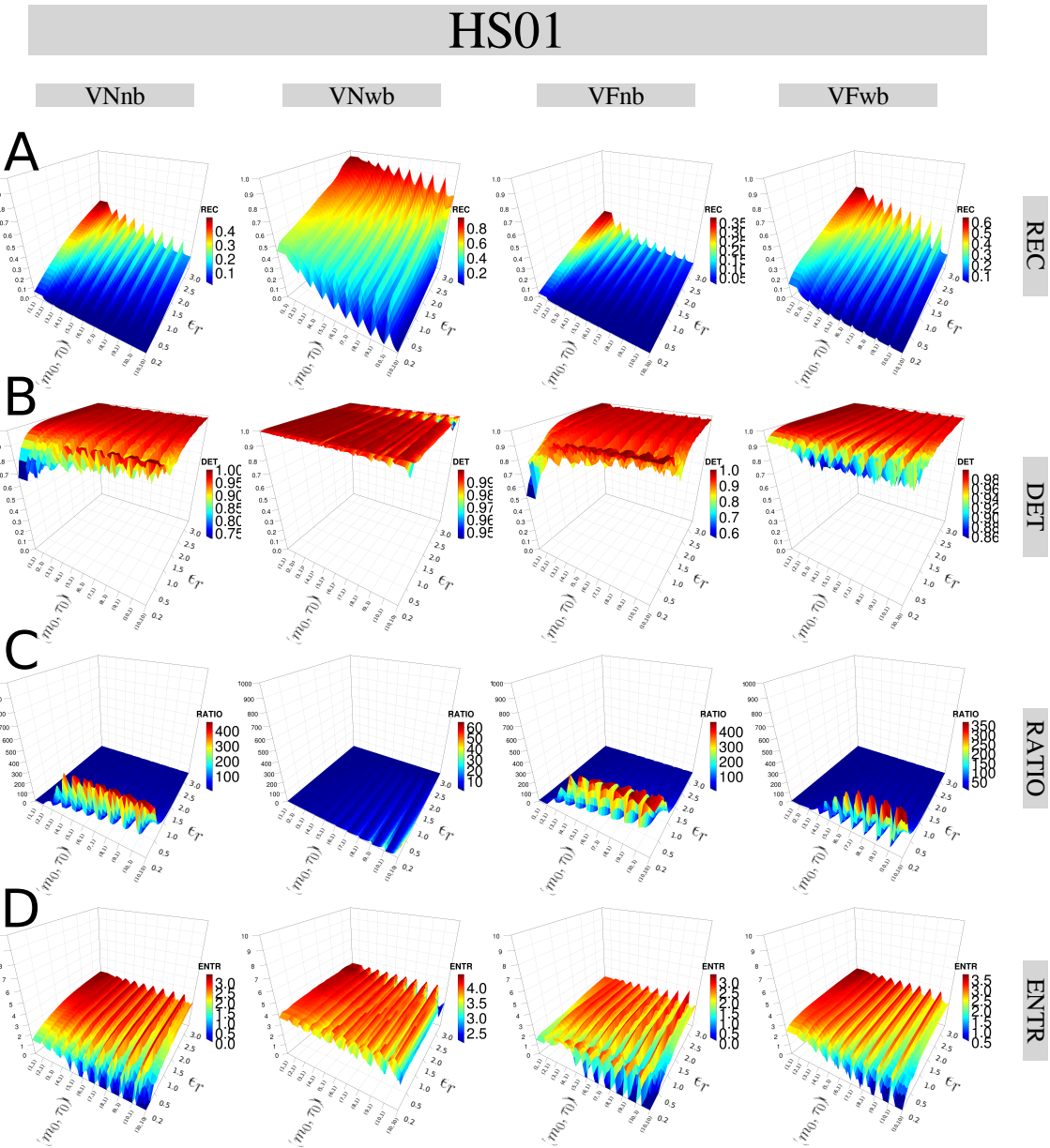


Fig. 5.18 **3D surface plots of RQA metrics for vertical arm movements with HS01.** 3D surface plots for (A) REC, (B) DET, (C) RATIO and (D) ENTR values with increasing pair of embedding parameters ($0 \leq m \leq 10$, $0 \leq \tau \leq 10$) and recurrence thresholds ($0.2 \leq \epsilon \leq 3$). RQA metrics are computed with the time series of participant p01 for sensors HS01, vertical arm movements activities (VNnb, VNwb, VFnb, VFwb) and sg0zmuvGyroY axis with 10 seconds window length. R code to reproduce the figure is available at [\[link\]](#).

Quantifying Human-Image Imitation Activities

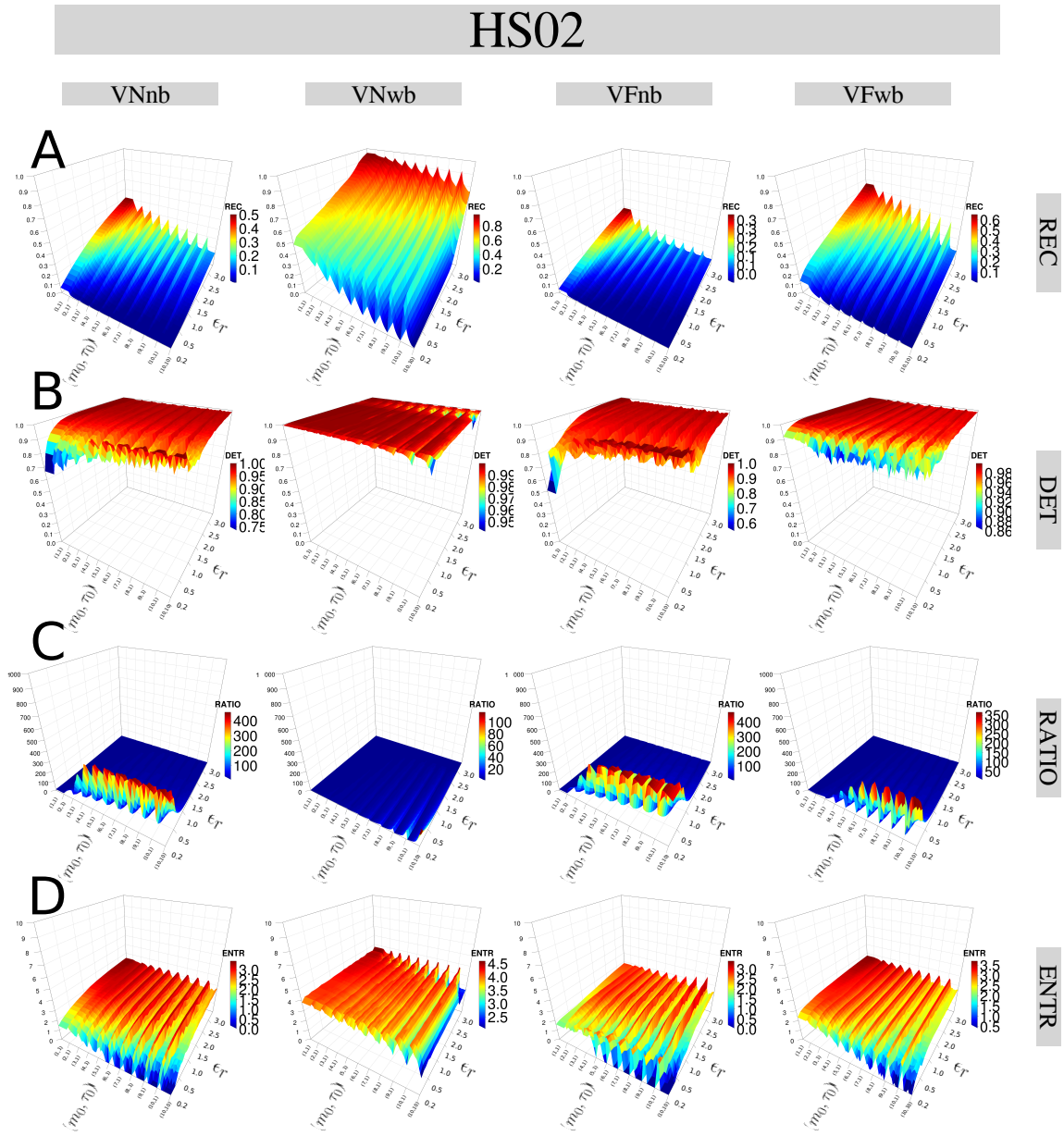


Fig. 5.19 3D surface plots of RQA metrics for vertical arm movements with HS02. 3D surface plots for (A) REC, (B) DET, (C) RATIO and (D) ENTR values with increasing pair of embedding parameters ($0 \leq m \leq 10$, $0 \leq \tau \leq 10$) and recurrence thresholds ($0.2 \leq \epsilon \leq 3$). RQA metrics are computed with the time series of participant p01 for sensors HS02, vertical arm movements activities (VNnb, VNwb, VFnb, VFwb) and sg0zmuvGyroY axis with 10 seconds window length. R code to reproduce the figure is available at [\[link\]](#).

5.7.2 Window size

3D surface plots of REC values with a short window length (2-secs) can affect the shape of 3D surface, however for window size of 5-sec, 10-sec and 15-sec, the 3D surface plots appear to show little changes (Figs 5.20(A)). For instance, one can see 3D surface plots of DET values with a window of 2 seconds window length is slightly different to other surface plots but keeping the plateau (red surface) in each of the surface plots (Figs 5.20(B)). Similarly, the 3D surface plots of RATIO values preserve the same plateau (blue surface) with little variations in the surface plots as window length is incrementing (Figs 5.20(C)). 3D surface plots of ENTR values appear to have similar aspects as the fluctuations of the curves keeps the same values (red and yellow colours). It can also be noted that the smoothness of 3D surface plots decrease as the embedding dimension parameters increase and such smoothness is also affected by the window length (see Figs 5.20(D)).

5.7.3 Smoothness

Figs 5.21 show the effects of three levels of smoothness (sg0zmuvGyroZ, sg1zmuvGyroZ and sg2zmuvGyroZ) in the RQA metrics. Generally, 3D surface plots from sg2zmuvGyroZ are affected by the smoothness. It can also be noted that REC values and ENTR values present a slightly different surface plots (see Figs 5.21(A, D)), while DET and RATIO values appear to be similar which is mainly reflected in the colour of the curves (see Figs 5.21(B, C)). In Figs 5.21(A), 3D surface plots for REC values tend be smoothed as the smoothness of the time series increase to the point where the increase of recurrence threshold affects the shape of the surface plots. Similarly, in Figs 5.21(D), 3D surface for ENTR values is affected by the smoothness of the time series to the point that the fluctuations in the surface does change drastically the shape by showing only an increase of ENTR values as the recurrence threshold increase.

Quantifying Human-Image Imitation Activities

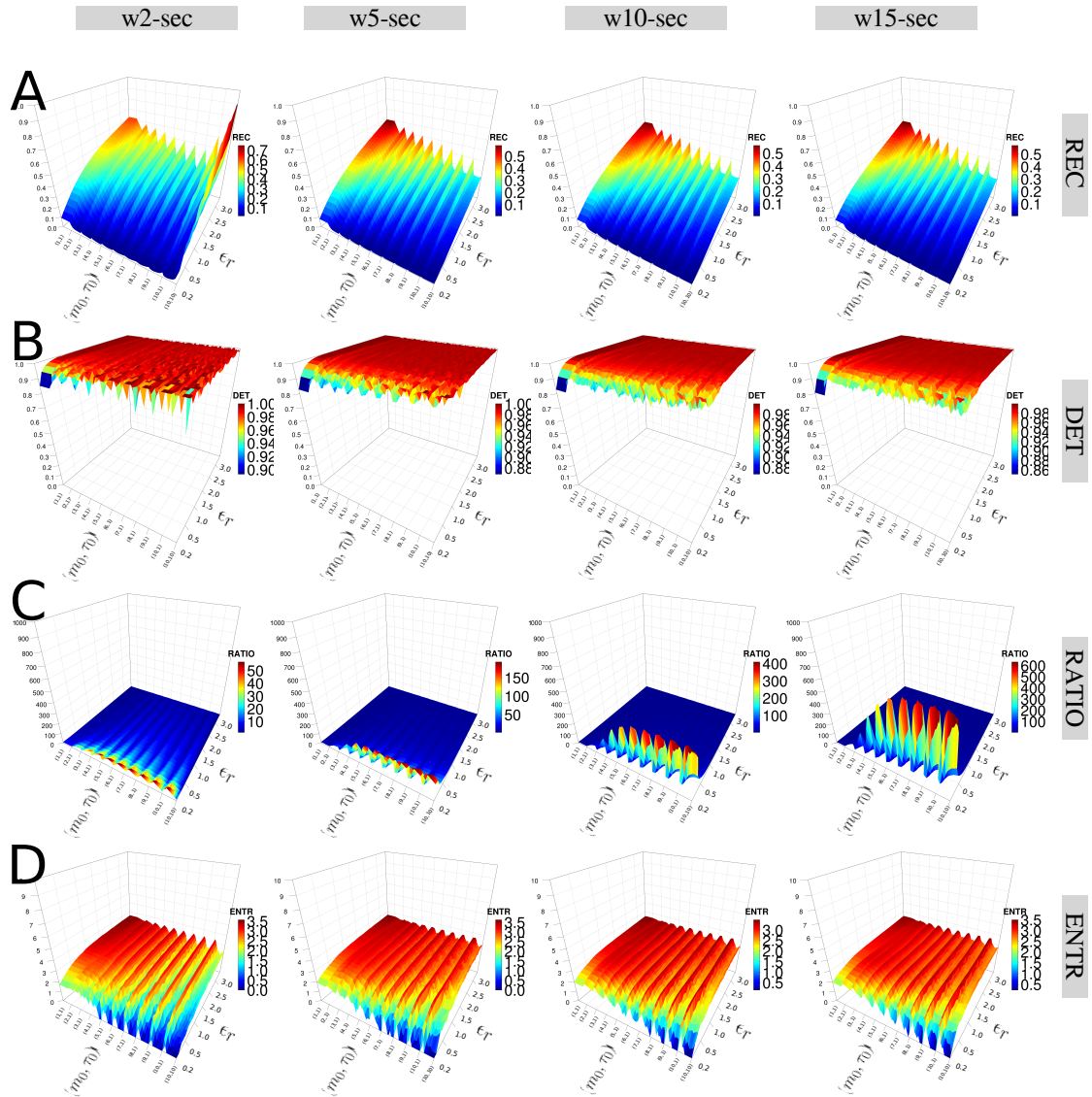


Fig. 5.20 3D surface plots of RQA metrics for different window lengths. 3D surface plots for four window lengths (w2-sec, w5-sec, w10-sec and w15-sec) and for (A) REC, (B) DET, (C) RATIO, and (D) ENTR values with increasing pair of embedding parameters ($0 \leq m \leq 10$, $0 \leq \tau \leq 10$) and recurrence thresholds ($0.2 \leq \epsilon \leq 3$). RQA metrics are computed with the time series of participant *p01* using HS01 sensor, HNb activity and sg0zmuvGyroZ axis. R code to reproduce the figure is available at [\[link\]](#).

5.7 Weaknesses and strengths of RQA

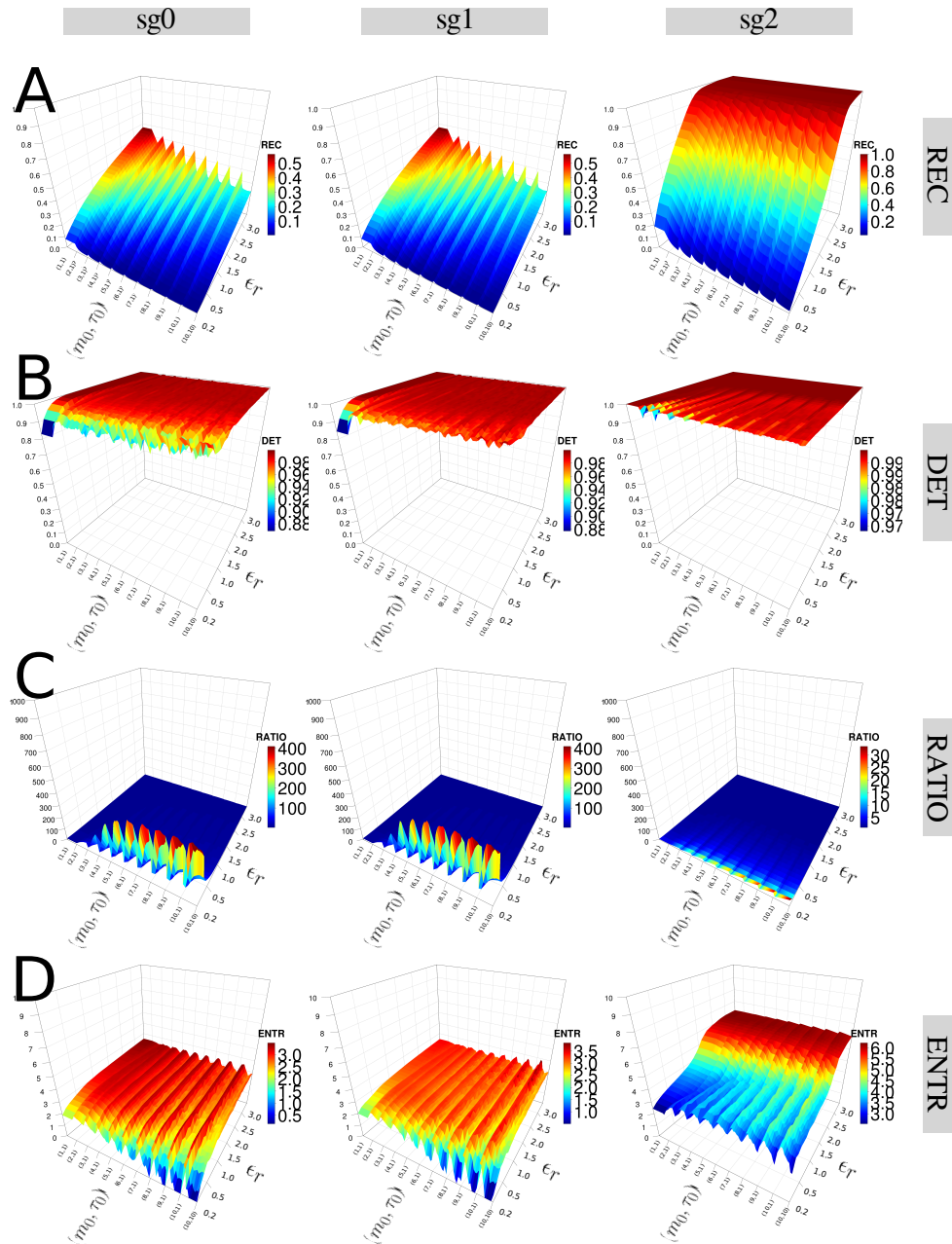


Fig. 5.21 3D surface plots of RQA metrics with three levels of smoothness. 3D surface plots for three levels of smoothness (sg0zmuvGyroZ, sg1zmuvGyroZ, and sg2zmuvGyroZ) and for (A) REC, (B) DET, (C) RATIO, and (D) ENTR values with increasing pair of embedding parameters ($0 \leq m \leq 10$, $0 \leq \tau \leq 10$) and recurrence thresholds ($0.2 \leq \epsilon \leq 3$). RQA metrics are computed with the time series of participant p01 with HS01 sensor, HNb activity and 10 seconds window length. R code to reproduce the figure is available at [DOI](#).

5.7.4 Participants

The shape of 3D surface plots of RQA metrics is also affected when using time series from different participants (Figs 5.22). For instance, 3D surface of DET values show slightly but noticeable differences in the fluctuations when embedding dimension and recurrence threshold increase (Figs 5.22(B)) which is similar for ENTR values where the fluctuations of the 3D surface plots changes for each of the participants (Figs 5.22(D)). However, the shape of 3D surface plots for RET values and RATIO values is little affected by the change of participants (Figs 5.22(A, C)).

5.7 Weaknesses and strengths of RQA

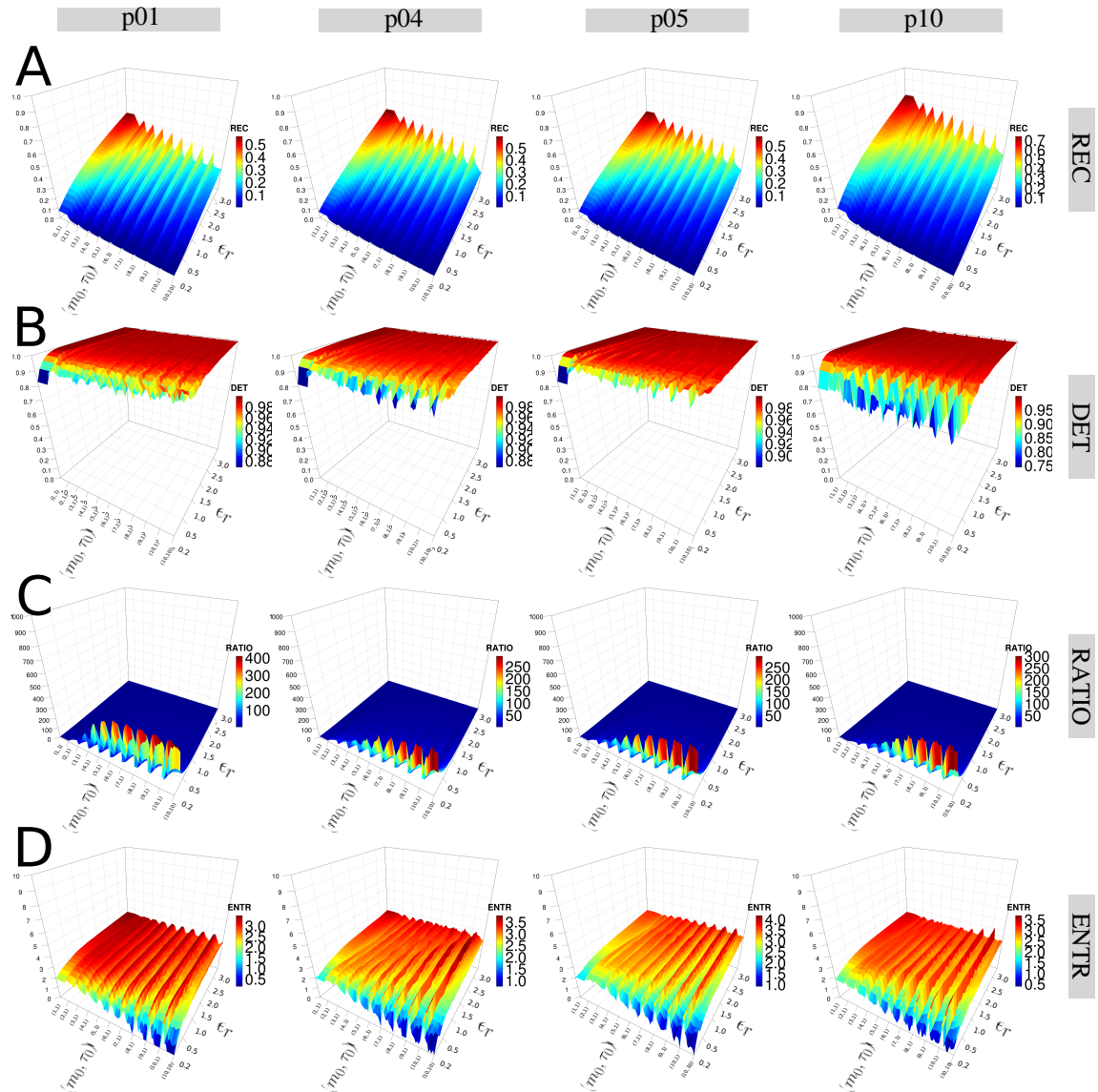


Fig. 5.22 **3D surface plots of RQA metrics with four participants.** 3D surface plots for participants $p01$, $p04$, $p05$ and $p10$ and for (A) REC, (B) DET, (C) RATIO, and (D) ENTR with increasing pair of embedding parameters ($0 \leq m \leq 10$, $0 \leq \tau \leq 10$) and recurrence thresholds ($0.2 \leq \epsilon \leq 3$). RQA metrics are computed with the time series of sg0zmuvGyroZ axis, HS01 sensor, HNnb activity and 10 seconds window length. R code to reproduce the figure is available at [\[link\]](#).

5.7.5 Final remarks

Different sources of time series (participants, sensors, activities, window length or level of smoothness) produce different results in nonlinear analysis methods (e.g. FNN, AMI, RSSs with UTDE, RPs and RQAs) and these results are sensitive to different parameters of nonlinear analysis methods (e.g., minimum dimension threshold, embedding parameters or recurrence thresholds). That said, 3D surface plots of RQA metrics with the variation of embedding parameters and recurrence thresholds appear to be helpful to understand the dynamics of any type of time series data. That is the case of 3D surface plots of ENTR values which with only the selection of variation of range of parameters (e.g., embedding parameters or recurrence thresholds), the 3D surface plots show clearly differences in the shape of 3D surface plots irregardless of the source of the time series. Hence, computing 3D surface plots of ENTR values with little parametrisation might be of help to understand the dynamics of human movement variability from different sources of time series data.